Ancestral radiation of paenungulate mammals (Paenungulatomorpha)-new evidence from the Paleocene of Morocco

Emmanuel Gheerbrant

ANCESTRAL RADIATION OF PAENUNGULATE MAMMALS (PAENUNGULATOMORPHA) - NEW EVIDENCE FROM THE PALEOCENE OF MOROCCO

Journal:	*Journal of Vertebrate Paleontology*
Manuscript ID	JVP-2022-0044.R4
Manuscript Type:	Article

Note: The following files were submitted by the author for peer review, but cannot be converted to PDF. You must view these files (e.g. movies) online.

Supplementary Data 4 - Analysis 1 MPTs.tre
Supplementary Data 5 - Analysis 2-1 MPTs.tre
Supplementary Data 6 - Analysis 2-2 MPTs.tre
Supplementary Data 3 nex matrix Hadrogeneios R4.nex

ARTICLE

Ancestral radiation of paenungulate mammals (Paenungulatomorpha) - New evidence from the Paleocene of Morocco

RH: GHEERBRANT—ANCESTRAL RADIATION OF PAENUNGULATA

ABSTRACT—Reported here is the discovery of a new mammal from the middle Paleocene of the Ouled Abdoun phosphate basin, Morocco. *Hadrogeneios phosphaticus*, gen. et sp. nov., is described based on dental and gnathic specimens. Comparative dental anatomy and CT scan observations support stem relationships to paenungulates. The cladistic analysis relates *Hadrogeneios* to paenungulatomorphs, especially based on the shared morphotypic condition of a dilambdodont ectoloph linked to inflated stylar cusps. Within the Paenungulatomorpha, *Hadrogeneios* is plesiomorphic not only with respect to crown paenungulates, but also to *Abdounodus* and *Ocepeia*, making it the basalmost known paenungulatomorph. *Hadrogeneios,* on the other hand, displays a peculiarly specialized mandibular symphyseal region (mentum), which is enlarged and raised high above the cheek teeth, and bears at its apex small incisors that are innervated and vascularized by a peculiar long and thin dorsal canaliculus. This is tentatively interpreted as a plier-like dental apparatus specialized for enhanced oral gripping function of the food, with increasing grip strength or enhanced grip precision. A composite reconstruction of the lower jaw of *Hadrogeneios phosphaticus*, based on 3D modeling from CT scans, is provided. *Hadrogeneios, Abdounodus* and *Ocepeia,* all from the same Ouled Abdoun Paleocene phosphate levels, are the very rare witnesses of the first evolution and diversification of the endemic African ungulates phylogenetically preceding the modern paenungulate orders.

LSID link: http://zoobank.org/pub:8A0974FB-6D0D-458C-A756-8D9C21B5AB98

SUPPLEMENTAL DATA—Supplemental materials are available for this article for free at www.tandfonline.com/UJVP

INTRODUCTION

Since the pioneering paleontological work of Camille Arambourg (e.g., Arambourg, 1952), the Ouled Abdoun phosphate basin in Morocco is most renowned for its rich marine vertebrate fauna found in several successive levels, extending from the latest Cretaceous to the early Eocene. Continental vertebrates were first discovered in 1996 in the Ouled Abdoun basin with the primitive proboscidean mammal *Phosphatherium* from Ypresian (early Eocene) phosphate levels (Gheerbrant et al., 1996). Discovery of mammals in the Paleocene levels of the Ouled Abdoun phosphate series was made later in 2001 (Gheerbrant et al., 2001; Gheerbrant, 2010). The Ouled Abdoun Paleocene mammals are the oldest known placentals from Africa, and all belong to African endemic taxa. Whereas the Ypresian phosphate levels yielded early representatives of modern orders of African ungulates (paenungulates), the Paleocene phosphate levels have yielded the first “condylarth-like” mammals, i.e., stem paenungulates, found in Africa, in addition to the earliest proboscidean *Eritherium* (see Gheerbrant, 2009 and Gheerbrant et al., 2012) and the earliest known hyaenodont *Lahimia* (see Solé et al., 2009). Most of these Paleocene mammals come from phosphate levels dated Selandian (Kocsis et al., 2014, 2016, 2021; Yans et al., 2014). The stem paenungulates described from the Paleocene of the Ouled Abdoun basin includes the two genera *Ocepeia* and *Abdounodus*, known by dental and cranial remains (Gheerbrant, 2010; Gheerbrant et al., 2001, 2014, 2016). *Ocepeia* belongs to a specialized lineage of stem paenungulates characterized by some anthropoid-like features such as a shortened and robust dentition (Gheerbrant, 2010; Gheerbrant et al., 2014). *Abdounodus* is

closer to the root of crown paenungulates, in particular with an incipiently quadritubercular upper molar pattern showing a developing metaconular hypocone (Gheerbrant et al., 2016).

Here is reported a new stem paenungulate (Paenungulatomorpha) from the Selandian phosphate levels, which is well distinct from *Ocepeia* and *Abdounodus*. It is characterized by very primitive features, but also by a remarkably specialized mandibular symphyseal region.

MATERIALS AND METHODS

Institutional Abbreviations—**MHNM.KHG**, Museum d'Histoire Naturelle de Marrakech (University Cadi Ayyad, Morocco), vertebrate collection from Khouribga sites (Ouled Abdoun phosphate series), Marrakech; **MHNT PAL**, Museum d'Histoire Naturelle de Toulouse, collections of paleontology, Toulouse; **MNHN,** Muséum national d'Histoire naturelle, Paris.

Material Studied—The holotype MHNM.KHG.227 was donated by N. Longrich to the collections of the Musée d'Histoire Naturelle de Marrakech (University Cadi Ayyad, Morocco). Other specimens, MHNM.KHG.224, MHNM.KHG.225 and MHNM.KHG.226, were donated by F. Escuillié to the same collections.

CT Scan, 3D Modelization, Software—All specimens studied here were subjected to X-ray Computed Tomographic (CT) imaging at the AST-RX platform of the MNHN, using a GE Sensing and Inspection Technologies phoenix|x-ray v|tome|x L240–180 CT scanner. I used the microfocus RX source 240 kV, detector 400 × 400 mm with a matrix of 2024 pixels (pixel size: 200 × 200 mm). Supplementary Data 1, Table S1 summarizes the scan parameters of the studied specimens.

Data were reconstructed using datos|x reconstruction software (Phoenix|x-ray, release 2.0) and then exported into a 16 bits TIFF image stack of 1537 (MHNM.KHG.225 and MHNM.KHG.226) and 1925 (MHNM.KHG.224 and MHNM.KHG.227) virtual slices in transversal view. MIMICS Innovation Suite software (Materialise, Research Edition, release 19–21) was used for the analysis, 3D modelling, and measurements on the 3D model. Corrections for reconstructions were also made with the help of the software VG studio Max Cinema 4D (Maxon, release 19–20).

The dental nomenclature used here follows Van Valen (1966). The tooth wear facets nomenclature follows that of Crompton (1971) and Schultz et al. (2018, 2020). For tooth orientation (anterior and posterior teeth), we use the terms “lingual” (medial side) and “labial” (lateral side) following classical and widely used comparative dental anatomical studies of mammals such as Van Valen (1966).

Cladistic Analysis—The cladistic analysis was made with TNT 1.5 (Goloboff & Catalano, 2016). The character matrix analyzed, which includes 38 taxa and 209 characters, corresponds to that of Gheerbrant (2009) and Gheerbrant et al. (2021), with few corrections and additions. The main changes in the matrix analyzed here correspond to the replacement of the taxon Sirenia by the three following stem genera: *Prorastomus*, *Pezosiren*, and *Eotheroides*. Their character coding, especially for *Pezosiren*, is based on Domning (2001, in press) and Domning et al. (2017). The phylogenetic matrix also includes some suprageneric taxa, the content of which is explained in Supplementary Data 2. Among them the Eutheria is used as outgroup taxon in the analyses. The matrix included nine uninformative characters and 48 additive characters that are listed in Supplementary Data 2. The uninformative

characters were inactivated before the analyses (xinact command of TNT). The character numbering scheme used in the description of the resulting most parsimonious trees (MPTs) starts from 0 (default option in TNT). Several analyses were developed: standard (unweighted) analysis, and two analyses imposing a scaffold to constrain the monophyly of the clade Afrotheria, one including the new species described here in Afrotheria, the other without it (Supplementary Data 2). We used the TNT command “force” for the constraining analyses (Supplementary Data 2). All analyses provide congruent results for the relationships of the new species described here (same topology for the Paenungulatomorpha). The analyses were made with the Traditional Search command and using the TBR swapping algorithm (number of replicates 10, tree saved per replicate 100, memory 10000 trees). For these analyses, the default collapsing rule was changed to “max. length = 0”. When some replications overflowed, a second round of TBR was conducted. Details on phylogenetic analyses are provided in Supplementary Data S1. The phylogenetic matrix used here is provided as a “NEXUS file” in Supplementary Data 3.

GEOLOGICAL SETTING

The material studied here was collected in the phosphate quarries from the Ouled Abdoun basin, Morocco. The geographical, geological and stratigraphic context of the Ouled Abdoun phosphate series and the fossiliferous sites are described in Gheerbrant et al. (2003), Kocsis et al. (2014), and Yans et al. (2014). The fossils were collected by local people from unknown exact sites in Ouled Abdoun

basin, but mostly from the quarrying area of Sidi Chennane (Yans et al., 2014). Their stratigraphic provenance is most likely from middle Paleocene phosphate beds. This is supported by a recent geochemical study by Kocsis et al. (2021) of the phosphate matrix of the studied mammal specimens, which shows that they have the chemostratigraphic signature of phosphate levels of the interval between the top of Bed IIb and the base of Bed IIa (chemostratigraphic Horizons 6–8 in Kocsis et al., 2021), corresponding to the Selandian–early Thanetian (middle–late Paleocene) interval. This interval includes the Selandian *Eritherium* bone-bed which has yielded most of the Paleocene mammal fossils discovered from the Ouled Abdoun phosphates series (Kocsis et al., 2014, 2021; Yans et al., 2014).

SYSTEMATIC PALEONTOLOGY

AFROTHERIA Stanhope, Waddell, Madsen, De Jong, Hedges, Cleven, Kao, Springer, 1998

PAENUNGULATOMORPHA Gheerbrant, 2016

FAMILY INCERTAE SEDIS

HADROGENEIOS, gen. nov.

Etymology—From the Greek *hadros*, well-developed, bulky, stout, ripe, large, strong, great; and *geneion*, chin: literally “strong chin” in reference to the large anterior part (mandibular symphyseal region and pars incisivus) of the dentary.

ZooBank Life Science Identifer (LSID)—zoobank.org:act:7AB6F6F4-DCEB-4678-B74F-1C0831CD39BE

Type [and Only] Species—*Hadrogeneios phosphaticus*, sp. nov.

HADROGENEIOS PHOSPHATICUS, sp. nov.

(Figs. 1–10; Supplementary Data 7–9)

Etymology—phosphaticus, in reference to its provenance from the phosphate beds of the Ouled Abdoun basin, Morocco.

Zoobank Life Science Identifer (LSID)—zoobank.org:act:0D3F474B-3192-4902-B7C9-EEC5CF9DB8EB

Type Locality and Age—Phosphate quarries of the Ouled Abdoun phosphate basin, Morocco, unknown exact locus. Phosphate Bed IIa, Paleocene, Selandian–early Thanetian. This age in supported by field data and geochemical analysis of the matrix of three paratype specimens MHNM.KHG 224, 225, and 226 (see Kocsis et al., 2021:fig. 6).

Holotype—MHNM.KHG.227, partial left dentary preserving the mandibular symphysis, the alveoli for two incisors, c1, and p1–3, and the teeth p4 and m1; in addition, a broken isolated left m3 is associated with the dentary.

Paratypes—MHNT PAL 2006.0.19, fragment of right dentary with m3; MHNM.KHG.223, isolated right M3; MHNM.KHG.224, right dentary broken into three pieces, including the mandibular symphysis; it preserves p3–4, m2, and the alveoli for p1, c1, and i1–3; MHNM.KHG.225, fragment of left dentary with m2–3; MHNM.KHG.226, fragment of right maxillary bearing strongly worn M2–3, and an associated isolated left M3 of the same individual.

Diagnosis—Stem paenungulate having an anterior lower dentition elongated with three distinct diastemata. The morphology of the mandibular symphyseal region

and pars incisiva is distinctive and autapomorphic among Paleogene placentals with the following features: symphyseal region large, robust and high; pars incisiva and mandibular symphysis enlarged, forming a prominent antero-dorsal process that is raised well above the check teeth and bears small incisors and a large canine. Lower incisors small; p1 single-rooted or partially two-rooted; p3 elongated and sharp; p4 almost fully molariform. Lower molars: bunodont crown, but sharp and crescentiform crests that outline a selenodont pattern; paraconid inflated and lingual; hypoconulid cuspidate, shifted lingually close to the entoconid; entolophid and hypolophid absent. Upper molars: stylar cusps and stylar shelf well developed; ectoloph sharp and dilambdodont (selenodont), linked labially to a large mesostyle and a large and bulbous stylocone; protocone large, low, and bunodont, surrounded by a thin lingual cingulum; conules and hypocone absent.

Description

Upper Dentition—Only M2–3 are known **(**Fig. 1; Supplementary Data 1, Fig. S1, Table S2**)**. MHNM.KHG.223 and MHNM.KHG.226 preserve respectively M3 and M2–3. Upper molars have three simple roots. The occlusal outline of the crown is triangular and extended transversely. The stylar shelf is wide and more markedly in the parastylar area. The ectoloph is typically dilambdodont (selenodont pattern), with a long labially deflected centrocrista that is linked to a large mesostyle. Preparacrista and postmetacrista (absent in M3) are also long and sharp. The ectoflexus forms a distinct notch on the labial side. The ectocingulum is present. Large inflated stylar cusps are present; they are by size order the stylocone, the mesostyle and the cusp D (variable). The hook-like parastyle is crestiform and mesially protruding (forming

the parastylar area). It bears on the mesiolabial side a wide parastylar groove (for the protoconid occlusion) extending transversely along the preparacrista and paracone. The stylocone is bulbous and it is the largest stylar cusp, being only a little smaller than the metacone. It is linked to the preparacrista. The mesostyle is large and widely linked to the centrocrista. In labial view, it is located between the paracone and metacone level, and not transversely aligned with the metacone. A stylar cusp D is distinct and inflated in the M2 of MHNM.KHG.226. The stylar cusp E (metastyle) is crestiform and small in M2; it is absent in M3. The postmetacrista links the cusp E in the M2 of MHNM.KHG.226. Accessory small stylar cuspules are present on the labial cingulum (ectocingulum). A distinct metacingulum extends below the metacone and postmetacrista in M2 (MHNM.KHG.226); it is less extended labially in M3 (MHNM.KHG.223, MHNM.KHG.226). Paracone and metacone are similar in size and deeply separated at the base. The conules are weak or absent. Only a tiny paraconular prominence is seen on the preprotocrista. The protocone is large, low, and wide mesiodistally. In lingual view it appears slightly canted mesially. The labial flank (in protofossa) of the protocone is flat. The protocone is surrounded by a precingulum and a postcingulum, which are lingually continuous in MHNM.KHG.223, but not in MHNM.KHG.226. Both end lingual to the paracone and metacone level. The hypocone is absent. The enamel is wrinkled in MHNM.KHG.223.

Wear Pattern (attrition and abrasion). Preparacrista, postparacrista and premetacrista show well developed crescentiform wear facets (facets 3–4 of Crompton, 1971), facets Me-M and P-ad of Schultz et al. (2018). They result from a shearing with labial crests of hypocone and protocone and correspond to a selenodont pattern. Tooth abrasion is extensively developed in MHNM.KHG.226 (an old individual), exposing widely the dentine at the level of the paracone, metacone,

protocone, centrocrista-mesostyle, and preparacrista. There is a wear facet on the preparacrista (facet 1 or PA-m), on the postmetacrista (facet 2 or ME-dl), and on the mesial flank of the protocone (facet 5 or PR-m).

The length of M2–3 in MHNM.KHG.226 is 11.96 mm; measurements of individual teeth are provided in Supplementary Data 1, Table S1.

Lower Tooth Row and Dental Formula—The tooth row and dental formula were described and reconstructed with the help of the digital modeling made from the CT scans of the available material. Measurements are provided in Supplementary Data 1, Tables S3–4.

The reconstructed lower dental formula is 3i–c–4p–3m, corresponding to the primitive placental dental formula. One specimen, MHNM.KHG.227, shows the presence of a small additional alveolus between p2 and p3 (Figs. 2, 6, 7). It is interpreted as a residual alveolus of a deciduous premolar, probably dp3, in the course of resorption. The alternative interpretation not retained here would be to identify this tooth as a remnant of an additional premolar inherited from the ancestral five premolars eutherian dental formula, i.e. as a dp3 followed by p4–5 (instead of p3–4), a tooth locus that is thought to be lost in the Placentalia (e.g., O'Leary et al., 2013). The interdental length between p2 and p3 (2.3 mm) in MHNM.KHG.227 closely matches that of the diastema between these teeth in MHNM.KHG.224 (see Table S2), supporting that it is the residual alveolus of a deciduous tooth that is resorbed in MHNM.KHG.224. Specimen MHNM.KHG.227 shows therefore that the dp3 was probably the last deciduous tooth to be shed in the species. It was lost late, after all permanent premolars and m1 were erupted, i.e., at the adult or subadult stage. There are three postcanine diastemata. The longest is between p1 and p2, followed by the slightly smaller one between p1 and c, and by the shortest between

p2 and p3. As a result, the anterior lower tooth row is elongated, in sharp contrast to *Ocepeia*.

Lower Incisors and Canines—Although not preserved, the incisors are represented by their alveoli in specimens MHNM.KHG.224 and MHNM.KHG.227 (holotype) (Fig. 7; Supplementary Data 1, Fig. S3). MHNM.KHG.224 shows the presence of three tiny incisors (Length of i1–3 = 4.4 mm) with short root (alveolus) (Fig. 7D–F). In the holotype only two incisor alveoli are preserved (Fig. 7A–C); one of the two anterior incisor alveoli (for i1–2) is broken, corresponding either to i2 or to i1. Judging from the alveoli, the incisors were closely appressed to each other, anterior to the canine.

The CT scans show that the incisors are innervated and vascularized by a very thin and long dorsal canaliculus that rises very high from the mandibular canal in the anterior part of the dentary bone with a course parallel to that of the canine root (Figs. 7–8; Supplementary Data 1, Fig. S3). Although only two incisor alveoli are preserved in MHNM.KHG.227, three dorsal canaliculi are present, confirming the presence of three teeth anterior to the canine (Fig. 7A–C). The dorsal canaliculus of i3 detaches earlier (more distally) from the mandibular canal than those of i1–2, and the latter separate very high, shortly below the tooth alveolus (Fig. 8); as a result, the dorsal canaliculus of i3 is much longer that those of i2 and i1. The CT scan section (Supplementary Data 1, Fig. S3) of MHNM.KHG.224 shows that i3 alveolus is smaller than that of i1–2, and that it has a subcircular section, whereas i1–2 have a more laterally compressed alveolus. i3 is located on the labial side of the lower jaw and closely wedged between the canine and the more lingually placed i2. In addition, MHNM.KHG.224 shows that i3 has a subvertical root, whereas the roots of i1–2 are more canted anteriorly.

A large alveolus indicates the presence of a large canine, which strongly contrasts with the small size of the incisors (Fig. 8; Supplementary Data 1, Fig. S3). The root of the canine is very large, deep and anteriorly canted (at about 45°), in a similar orientation to the incisors. According to the alveolus, it was located anteriorly, close to the incisors, and very labially. In MHNM.KHG.224, it has the labial border lower than the lingual border; as a result, the canine might have been asymmetric and more exposed labially (labially higher crown).

Lower Premolars—There are four premolars (p1 and p2 being known only by their alveoli).

According to its alveolus, p1 is the smallest cheek tooth (Supplementary Data 1, Table S4), but it is larger than the incisors. It is separated from the canine and p2 by diastemata. The p1 is either entirely one-rooted with a simple root (MHNM.KHG.227) or one-rooted with a bifid root apex (MHNM.KHG.224). The 3D digital model of the alveolus of p1 in MHNM.KHG.224 (Fig. 7) shows a single main root which separates in two at its apex. It corresponds either to an intermediate structural state from an ancestral two-rooted p1 or to a root which is beginning to divide in this species. In any case, the root of p1 is robust and relatively longer than those of other premolars (Figs. 6–7).

According to its alveoli, p2 is only slightly smaller than p3. The latter, preserved in MHNM.KHG.224, is an elongated, narrow, and high tooth bearing sharp cusps and crests; its crests are more or less mesiodistally aligned. It has a simple trigonid and a small unicuspid talonid. It bears a strong and high anterior paraconid, which is a little higher than the talonid. The main, and by far larger, cusp is the protoconid. The smallest cusp is the hypoconid, which is located labially.

The p4, preserved in MHNM.KHG.224, is a nearly fully molariform premolar. It is larger than p3 and about as long as m1. It bears very small precingulid and ectocingulid. The trigonid is typically elongated with respect to the molars. It is narrower than the talonid. It bears a strong and high paraconid that is mesially and labially located, in front of the protoconid. The paracristid is mostly mesiodistal and labially placed. The metaconid is well inflated and is located lingually, at a slightly more distal level than the protoconid. In MHNM.KHG.224, the mesial root of p4 is longer than the distal one and it is a little canted posteriorly (root apex more anterior). The talonid is molariform with the presence of a deep basin (postfossid) surrounded by three well inflated cusps of similar size, the hypoconid, hypoconulid and entoconid. The postfossid (talonid basin) is widely and deeply open lingually. By contrast to the molars the three talonid cups in p4 are approximated to each other, the hypoconulid being distal and slightly closer to the hypoconid. The cristid obliqua is well developed. It rises lingually on the trigonid, behind the metaconid.

Lower Molars—Lower molars have a moderately bunodont crown. The labial cusps and crests are sharp and bear developed crescentiform shearing wear facets, drawing a selenodont pattern. The crown is inflated above the roots, especially on the labial side. The labial cusps, protoconid and hypoconid, are the largest ones; their lingual flank is convex and bulging as a distinctive vertical carina. The molars bear a more or less distinct and continuous labial cingulid that extends from the mesial flank of the trigonid to the distal flank of the talonid. There is a radicular groove on the internal side of the roots.

The trigonid is a little higher than the talonid and of overall comparable width. It is not compressed but more or less elongated. The precingulid is weak or absent. The paraconid is well developed, cuspidate, and it is only slightly lower than the

metaconid. It has a distinct mesiolingual crest that projects mesially from the trigonid. This crest links a small but well distinct parastylid (= “cusp e” in therian terminology) which is bulging on the mesiolingual angle of the molars. The paracristid and protocristid are sharp and high and they are arranged in a selenodont pattern. The paracristid is slightly convex mesially. The protoconid is the largest cusp, but it is low and only a little higher than the paraconid and metaconid. The metaconid is distally located with respect to the protoconid, and more so from m1 to m3. The prefossid (trigonid basin) is widely open lingually. The metaconid bears a distinct postmetacristid and a metastylid.

The talonid is as long as, or longer than, the trigonid. Its relative length increases from m1 to m3. The ectoflexid is shallow and wide. The talonid notch is wide and deep. The cristid obliqua is long and sharp. In most specimens it joins the trigonid at its mid width, below the protocristid notch, and it does not rise high on it; in MHNM.KHG.225 it ends slightly more lingually, below the metaconid apex. The cristid obliqua bears a small mesoconid at its mesial part. The postcristid is also long. It joins a hypoconulid that is shifted lingually and closely approximated to the entoconid. As a result, the hypoconid and entoconid are “twinned” and the hypoconid and hypoconulid are separated by a wide notch on the postcristid. The hypoconulid is a little smaller than the entoconid. The entoconid lacks an anterior crest (i.e., no entocristid). When the labial cingulid is distinct, it extends distolingually to the level of the hypoconulid. There is no entolophid or hypolophid.

The m1 is slightly smaller than m2, and m2 is slightly wider than m3 (Supplementary Data 1, Table S4). The paraconid is more lingual on m2 and m3. The m3 is characterized by a much longer talonid than the trigonid. The distal root of m3 is classically elongated and compressed laterally with respect to the mesial one.

Individual variation. The most remarkable variable morphological traits are the p1 that is either one rooted (MHNM.KHG.227) or partially two rooted (roots separated at apex in MHNM.KHG.224), and the residual dp3 alveolus that is retained in one specimen (MHNM.KHG.227) at subadult stage. The relative width of the talonid is variable, especially on m3. A larger talonid than trigonid in m3 is seen on MHNM.KHG.224, whereas it is subequal to trigonid on MHNM.KHG.227. The development of the labial cingulid and the ectostylid is variable in the material: it is absent in MHNM.KHG.225, and present in MHNM.KHG.227 (m3, with ectostylid), MHNM.KHG.224 (m2), MHNT PAL 2006.0.19 (m3). The m3 of MHNM.KHG.227 has an inflated ectostylid. m2 and m3 of MHNM.KHG.225 have a cristid obliqua that ends in the lingual part of the trigonid, whereas the cristid obliqua ends at trigonid mid-width in other specimens. The m3 of MHNT PAL 2006.0.19 and MHNM.KHG.227 lacks distinct parastylid.

Wear pattern (attrition). The lower jaw specimens here described belong to subadult individuals with poorly worn teeth. Attrition wear facets are, however, well seen. Crescentiform labial shearing wear facets are present on the protocristid (wear facet 1 of Crompton, 1971, wear facet prod-d of Schultz et al., 2018, 2020) and paracristid (wear facet 2, pacd-mb). In addition, there are shearing wear facets on the cristid obliqua (wear facet 3, hy-mb) and the postcristid (wear facet 4, hy-l). Distinct wear striae are seen especially on wear facets 1 and 2; they are inclined at 40° to 25° with respect to the horizontal plan. A wear facet is present on the lingual flank of the twinned hypoconulid and entoconid (facet 6, Ed-Mb). Measurements of lower jaw and teeth of *Hadrogeneios phosphaticus*, gen. et sp. nov. are provided in Supplementary Data 1, Tables S2–5.

Dentary—One remarkable feature of the described material is the enlarged and high mandibular symphysis as shown by the holotype and MHNM.KHG.224, in which the symphyseal region and the pars incisiva are greatly developed and expanded high, forming a prominent antero-dorsal process. Between p1 and p2, the anterior tooth row rises high above the molar occlusal plane at an angle of about 40–45°. As a result, the incisors are located well above the cheek teeth, at the apex of a strong and high symphyseal region (Figs. 2B–C, 3B–C, 7, 9; Supplementary Data 1, Fig. S3A). The pars incisiva and the symphysis are consequently significantly higher and deeper (mandibular symphysis height: 27 mm from base to apex in MHNM.KHG.224), by almost twice the height, than the mandibular corpus (height of corpus = 10–15 mm below m2). A peculiar endostructural feature (CT scan observation) linked to the enlarged and high symphyseal region is the very long and thin dorsal canaliculi (Figs. 7–8; Supplementary Data 1, Fig. S3) connecting the incisors (pars incisiva), which are located high, at the apex of the prominent vertical process of the mandibular symphysis. The symphysis is flat. There is no evidence of a fused symphysis in the described material that is represented by subadult specimens with poorly worn teeth. However, it is not excluded that such a large and flat mandibular symphysis was fused in older individuals. The structure combining small incisors (but large canine) with a strong and high mandibular symphyseal process is remarkable. This morphology indicates a specialized, possibly pliers-like, anterior dental apparatus that is adapted for a particular oral gripping function of the food, with increasing grip strength or enhanced grip precision.

The mandibular symphysis extends posteriorly to the level of p1 (MHNM.KHG.227) or below the diastema between p1–p2 (MHNM.KHG.224). A distinct ventrolateral crest (MHNM.KHG.224, MHNM.KHG.227) for strong muscular

attachment runs on the corpus back from the mandibular symphysis to below the level between p4 and m1 (Figs. 2B, 3C, 7A, D; Supplementary Data 1, Fig. S4). This is likely the crest for the genioglossus muscle that is involved in the protraction of the tongue (McClung & Goldberg, 2000). The remarkable development of this bony crest in the Ouled Abdoun species suggests a long tongue firmly attached anteriorly, in close relation to the strong mandibular symphysis. The mandibular corpus is not deep below the teeth (corpus height about three times the molar height), and it is flattened on the labial side and slightly inflated (convex) on the lingual side. Two mental foramina of similar size are present. The posterior one is located below the diastema between p2–p3. The anterior one is just behind the canine. The vertical ramus, represented by part of masseteric and coronoid crest, rises labial to the m3 talonid (Fig. 3E–F). The masseteric crest is well developed and sharp, and it extends on the corpus well below the alveolar border. Behind m3, the coronoid crest and the sharp masseteric crest delimit a coronoid fossa on the ramus. The CT scan observation confirms that there is no coronoid foramen, unlike paenungulates. The remnant of the coronoid process seen in MHNM.KHG.225 is slightly canted posteriorly, in contrast to *Phosphatherium* where it is canted anteriorly. The subcondylar notch is distinct on MHNM.KHG.225. It is located at a low level of the mandibular corpus, much lower than in *Ocepeia*. Its position is closer to *Abdounodus*, but still lower. In addition, the neck of the mandibular condyle diverges from the ramus below the alveolar plane. This means that the mandibular condyle was low, close to the tooth row level. The mandibular foramen seen in MHNM.KHG.225 is located right below the alveolar plane, and 9 mm behind the m3. Mandibular measurements are provided in Supplementary Data 1, Table S5.

Comparisons

The new Ouled Abdoun material described here is characterized in this study as belonging to a new genus and species that is named *Hadrogeneios phosphaticus*, gen. et sp. nov. Its comparison with early Paleogene placental mammals shows the closest morphological affinity with the stem paenungulatomorph *Ocepeia daouiensis*, which comes from the same Paleocene levels of the Ouled Abdoun basin (Gheerbrant et al., 2001, 2014; Gheerbrant, 2010). The resemblance in molar morphology is the most noticeable. However, *Hadrogeneios phosphaticus* departs from *Ocepeia* in the derived and likely autapomorphic construction of the strong mandibular symphyseal region (mentum), in which the symphysis and the pars incisiva are enlarged and raised above the cheek tooth row.

This is combined with a suite of other distinct features that are primitive, such as some important molar features and the full placental dental formula with the retention of the two first premolars (p1–2) in contrast to *Ocepeia*.

An enlarged symphyseal region is known in some early Paleogene mammals. This is the case of the arctocyonid “condylarth” *Anacodon ursidens* Matthew and Granger, 1915, from the early Eocene of Wyoming (U.S.A.). However, the construction of the symphyseal region of *Anacodon* is quite different: it is not enlarged in its upper part but in its lower part, forming a mandibular flange similar to the mandibular morphology known in carnivores with large, compressed sabre-like upper canines (e.g., machairodonts). This is not homologous to the morphology of *Hadrogeneios phosphaticus*. In addition, the dental morphology of *Anacodon* is well distinctive from that of *H. phosphaticus*. This is also true for other non-carnassial Paleogene taxa that have a mandibular flange and an enlarged upper canine such as uintatheres (*Bathyopsis* and *Uintatherium*) and astrapotheres (see Kramarz et al.,

2019). Comparisons show that the anterior part of the dentary of *H. phosphaticus* is instead derived in a specialized functional way for a distinctive mode of ingesting food.

The most remarkable shared dental trait of *Hadrogeneios* and *Ocepeia* is the incipient but well-distinct selenodont pattern. In the upper molar, the selenodont pattern is displayed by the dilambdodont ectoloph that is linked to strong stylar cusps such as the mesostyle and stylocone. In the lower molars, the selenodont pattern is seen in the sharp and long labial crests (protoconid and hypoconid crests), bearing crescentiform wear facets. This specialized pattern shared with *Ocepeia* is associated to a similar general tooth morphology such as the bunodont crown. The upper molar morphology affinity of *Hadrogeneios* and *Ocepeia* is remarkable not only in the dilambdodont pattern. It also lies on the occlusal outline, the wide stylar shelf bearing inflated stylar cusps, the large parastyle, the presence of a metacingulum, and the massive protocone that is low, bunodont, and surrounded by a well-developed lingual cingulum. Lower molars of *Hadrogeneios* and *Ocepeia* share other characters such as a high and cuspidate paraconid, presence of postmetacristid, and the convex lingual flank of lower cusps. The dentary shares the presence of a lower bony crest running on the ventral rim of the anterior part of corpus (crest for genioglossus m.), the masseteric crest extended below the tooth row, and the presence of a coronoid fossa. The zygomatic apophysis of the maxilla similarly diverges between M2 and M3.

These shared features of *Hadrogeneios* and *Ocepeia* argue for taxonomic affinity, possibly at the familial level. The cladistic analysis recovers a basal relationship of *Hadrogeneios* to stem paenungulates such as *Ocepeia*, but in a paraphyletic position that refutes its familial allocation to the Ocepeiidae (see below).

Hadrogeneios departs indeed from *Ocepeia* in a number of significant features. It differs most remarkably in the enlarged and robust anterior part of the dentary (mandibular symphysis and pars incisiva), in the tooth row that is contrastingly elongated with three distinct anterior diastemata and with a full placental dental formula (four premolars), and in the much lower bunodonty of p3–4 and molars. *Ocepeia* has a much less developed chin and shorter dentary and tooth row. It also has a much higher articular condyle, a wider and rounded angular process, a more inflated corpus, and a stronger masseteric crest. The cheek teeth of *Hadrogeneios* are sharper than those of *Ocepeia*. In particular, the crown of lower molars is higher and raised vertically in contrast to *Ocepeia*, in which the labial flank of the crown is inflated at the base and lingually inclined. Lower molars of *Hadrogeneios* depart in many other characters. The most remarkable include the absence of entolophid and hypolophid, presence of parastylid, absence of entocristid related to the development of a wide and deep talonid notch, and the high hypoconulid that is twinned with the entoconid. Other differences from *Ocepeia* include the trigonid longer (not compressed), higher, and less canted mesially, the paraconid higher, sharper, and more lingual (anterior molars), the absence of premetacristid, the postmetacristid and mesoconid much smaller, the absence of entoconulid, the ectocingulid well differentiated, the absence of secondary cuspules on the postcristid, and the proportionally smaller m3, bearing less developed hypoconulid lobe. The premolars of *Hadrogeneios* are also very different from those of *Ocepeia*; p4 is submolariform in *Hadrogeneios,* whereas it is simple in *Ocepeia*; it has distinct paraconid, metaconid, talonid basin, and a large hypoconid. In addition, p3 and p4 are more elongated and sharper unlike the simple, shorter, and bunodont premolars of *Ocepeia.* The p1–2 are present in *Hadrogeneios* whereas they are lost in *Ocepeia*. Upper molars of

Hadrogeneios depart from *Ocepeia* in the absence of conules, the longer transverse occlusal outline with narrower protocone, the longer preparacrista, the stylocone much larger and well separated from the parastyle (fused with parastyle in *Ocepeia*), the larger and more hook-like parastylar area (M1–3), and the wider interdental space between molars. *Hadrogeneios phosphaticus* is 80–90% smaller in dental measurements than *Ocepeia daouiensis*, which is the smallest species of the genus.

Most of these differences unambiguously relate to the plesiomorphic morphology of *Hadrogeneios* with respect to *Ocepeia.* A remarkable exception is the specialized mandibular symphyseal region of *Hadrogeneios* with respect to *Ocepeia*. The much larger and robust mandibular symphysis and pars incisiva, forming a prominent high process that is raised well above the cheek tooth row, and bearing very small and crowded incisors innervated and vascularized by very long and thin dorsal canaliculus (Figs. 7–8; Supplementary Data 1, Fig. S3), all make a very peculiar anterior dental apparatus that is most likely autapomorphic in *Hadrogeneios*. This supports that *Hadrogeneios* documents a distinct new lineage of basal Paenungulatomorpha.

Abdounodus comes from the same Paleocene phosphate levels of the Ouled Abdoun basin as *Ocepeia* and *Hadrogeneios* (Gheerbrant, 2010; Gheerbrant et al., 2001, 2016). It shares with *Hadrogeneios* the presence of a diastema in front of p3, suggesting a more elongated tooth row in both genera than in *Ocepeia*. Other resemblances are the strong masseteric crest extending low on the corpus, the symphysis extended close to p2, the absence of a coronoid foramen (as also in *Ocepeia*), and the low position of the mandibular condyle with respect to the tooth row. *Abdounodus,* however, departs from *Hadrogeneios* in several specialized traits, that are also distinctive with respect to *Ocepeia.* The most noticeable are incipient

lophodont traits, such as the presence of a small hypolophid and the low cingulid-like postcristid (Gheerbrant, 2010; Gheerbrant et al., 2001, 2016). Other derived features of *Abdounodus* are the smaller molar talonid, the hypoconulid located much more labial, the much more bunodont teeth, and the smaller m3 (reduced in size with respect to m2). In addition, *Abdounodus* differs from *Hadrogeneios* by the simple (premolariform) p4 and the narrower mandibular corpus. The upper molars of *Abdounodus* are well distinctive from those of *Hadrogeneios* in derived traits such as the large and bulbous metaconule, the smaller parastyle, and the transversely narrow crown.

The upper molar pattern of *Hadrogeneios* in stylar area is remarkable. It has intriguing resemblance with some other taxa, which deserves comments and comparisons.

Outside paenungulatomorphs, it is surprisingly similar to cyriacotheriid pantodonts from the Paleocene of North America (see Scott, 2010) in the dilambdodont (= selenodont) ectoloph, which is linked to large and inflated stylar cusps (stylocone and mesostyle), and the well-developed stylar shelf. This is associated to a similar transversely extended occlusal outline and to the large and low protocone that is surrounded by a lingual cingulum. However, *Hadrogeneios* is well distinctive from the cyriacotheriids *Cyriacotherium* and *Presbytherium* in a number of important characters such as the absence of conules (present and large in *Cyriacotherium*), the narrower stylar shelf, the shorter postmetacrista, the smaller m3, and the much smaller size. The lower molars of cyriacotheriids have a shorter, more compressed occlusal outline (shorter and wider), a less bunodont and sharper morphology with higher crests and cusps, longer cristid obliqua, hypoconulid not twinned to entoconid, and absence of diastema between p3 and p2. The

dilambdodont ectoloph connected to stylar cusps is obviously convergent in *Hadrogeneios* and cyriacotheriids.

Comparison of the upper molar pattern of *Hadrogeneios* with advanced Adapisoriculidae, such as *Garatherium* (Paleocene of Morocco and Ypresian of Algeria), *Adapisoriculus* and *Remiculus* (Paleocene of France), is more intriguing and interesting (Supplementary Data 1, Fig. S5). These genera have a remarkably similar W-like dilambdodont ectoloph that is linked to a cuspate mesostyle, and they share some other interesting features such as the inflated stylar cusps, especially the mesostyle and stylocone, the wide stylar shelf, the large paracingulum, the metacone as large as the paracone, the occlusal outline wide transversely, and the large and hook-like parastylar area. In addition, the lower molars strikingly share the hypoconulid close to entoconid. However, *Hadrogeneios* differs from *Adapisoriculus* and *Garatherium* in the absence of conules, the lower and larger protocone, the presence of lingual cingulum, the narrower occlusal outline and stylar shelf, and the bunodont crown. *Remiculus* shares with *Hadrogeneios* peculiar traits, unknown in other adapisoriculids, such as an incipiently bunodont crown, the transversely narrower occlusal outline, the metacingulum present, the large (voluminous) protocone (unlike *Garatherium*), and the presence of a lingual cingulum.

The two Paleogene African insectivore-like placentals from the Fayum (Egypt), *Dilambdogale* (BQ−2, Birket Qarun Formation, late Eocene; Seiffert, 2010), and *Widanelfarasia* (L41 site, Jebel Qatrani Formation, earliest Oligocene; Seiffert et al., 2000), share upper molars with a dilambdodont ectoloph and well-developed stylar cusps. However, their ectoloph morphology is less specialized than in *Hadrogeneios*, with a much smaller mesostyle that is not linked to the ectoloph. In addition, they are distinctive in the wider stylar shelf, the mesiodistally narrow protocone, and the larger

paracone with respect to the metacone. Lower molars of *Dilambdogale* and *Widanelfarasia* differ in the small talonid basin, the hypoconulid not approximated to the entoconid, and the (relatively) smaller m3. *Dilambdogale* and *Widanelfarasia* have in fact a dental morphology that is quite reminiscent of the dilambdodont adapisoriculids.

PHYLOGENETIC ANALYSIS

The cladistic analysis recovers well-resolved MPTs that support a basal relationship of *Hadrogeneios* to *Ocepeia*, *Abdounodus*, and crown Paenungulata (Fig. 10). It indicates that *Hadrogeneios* is the basalmost known paenungulatomorph. In the standard analysis (Supplementary Data 2, Analysis 1; Supplementary Data 4), which recovers 180 MPTs (L [length] = 972 steps, RI [Retention index] = 34.8; CI [Consistency index] = 61.3), *Hadrogeneios* is indeed the sister group of all other paenungulatomorphs (consensus tree and majority rule tree) (Fig. 10). The node including *Hadrogeneios* and other paenungulatomorphs is supported by low Bremer support (BS = 1) and low Bootstrap score; this is related in part to the limited knowledge of *Hadrogeneios*, which is restricted to dental and mandibular features representing only 49% of all coded characters in the phylogenetic matrix. In the cladistic analyses developed here, *Hadrogeneios* is never recovered as sister group to *Ocepeia*. It belongs to a stem paenungulatomorph lineage that branches earlier than the Ocepeiidae.

Another cladistic analysis was developed, in which the monophyly of the clade Afrotheria is constrained (Supplementary Data 2, Analysis 2; Supplementary Data 5–6). When the position of *Hadrogeneios* is constrained within the Afrotheria, the resulting MPTs (30 MPTs found with L = 986) recovers it as the most basal stem

paenungulate; it is a stem paenungulatomorph, but not a stem afrotherian. Interestingly, the node including *Hadrogeneios* and other paenungulatomorphs is more robust in this constrained analysis (Bremer support BS = 4) than in the standard analysis (Supplementary Data 2, Analysis 1). When *Hadrogeneios* position is not constrained within the Afrotheria (itself constrained), it is recovered at the root of crown placentals together with *Todralestes* and *Ptolemaia* (Supplementary Data 2, Analysis 2), with a very low Bremer support.

The relationships of *Hadrogeneios* with other paenungulatomorphs in the unconstrained analysis is supported by five synapomorphies. They include a single exclusive synapomorphy, i.e. the presence of a coronoid (retromolar) fossa (character 62–1). Other shared features are homoplastic. The most important ones (i.e., less homoplastic) are the coronoid apophysis rising at m3 level (character 55–1, RI = 75), the inflated mesostyle (character 104–1, RI = 77), and the centrocrista strongly dilambdodont and linked to mesostyle (character 113–2, RI = 84). Here also the dilambdodont ectoloph linked to mesostyle is recovered as a major feature of the ancestral morphotype of the Paenungulata and Paenungulatomorpha (Gheerbrant et al., 2016). The resulting MPTs recovered from the cladistic analysis of *Hadrogeneios* recover a topology for paenungulates congruent with that previously published. In particular, *Eritherium* is the sister group to Proboscidea (Gheerbrant, 2009), and Embrithopoda are the sister group to crown Tethytheria (Gheerbrant et al., 2021).

DISCUSSION AND CONCLUSION

Hadrogeneios phosphaticus, gen. et sp. nov. is the third stem paenungulate lineage found in Africa, along with *Abdounodus* (*A. hamdii*) and *Ocepeia* (*O. daouiensis* and *O. grandis*) from the same Paleocene sites of the Ouled Abdoun phosphate basin (Morocco). *H. phosphaticus* remains partially known, only by teeth and jaws. The comparisons and phylogenetic analysis, however, do argue well that *H. phosphaticus* documents the most basal known paenungulatomorphs. Its dental morphology is remarkably primitive with respect to crown Paenungulata in the tritubercular upper molar pattern (no hypocone or pseudohypocone), the upper molars transversely wide and lacking conules, the retention of a lower molar paraconid as in *Ocepeia* and *Abdounodus*, the last molar not enlarged, the small lower incisors, the large lower canine, and the lack of a coronoid foramen. It is more plesiomorphic than the two other stem paenungulates *Ocepeia* and *Abdounodus* in the less bunodont teeth, the absence of a hypolophid, and the absence of a metaconule. Another noticeable distinctive dental trait of *Hadrogeneios* from *Ocepeia* and *Abdounodus* is the molariform last premolar. It is a possible autapomorphy in the cladistic analysis (character 22–1). On the other side, *Hadrogeneios* displays the derived upper molar morphology of stem and crown paenungulates (Paenungulatomorpha), with the presence of a dilambdodont W–like ectoloph linked to well-developed stylar cusps. This is a plesiomorphic (morphotypic) condition within Paenungulatomorpha and a derived condition within placentals, i.e., a paenungulatomorph synapomorphy. Within the Afrotheria, the polarity of the dilambdodont condition is ambiguous, because extant tenrecoidean insectivores (tenrecids, potamogalids, and chrysochlorids) are specialized in a divergent molar zalambdodont condition, in which the centrocrista is reduced. Other insectivore-like afrotherians, such as early macroscelideans, have a rectodont centrocrista.

Regarding the tubulidentates, the homology of their peculiar molar pattern remains unclarified. Despite these open questions on the ancestral afrotherian dental morphotype, when the position of *Hadrogeneios* is constrained to fall within the clade Afrotheria, it is recovered, with strong support, as a stem paenungulate and not as a stem afrotherian. Within Afrotheria, the W-like ectoloph linked to an inflated mesostyle is a key dental feature of the node Paenungulatomorpha, including *Hadrogeneios*.

As noted above, some adapisoriculids, such as *Garatherium* and *Remiculus*, share an intriguingly similar dilambdodont upper molar pattern. They also share a molariform p4 (e.g., *Remiculus*) and the hypoconulid approximated to the entoconid on lower molars (dilambdodont adapisoriculids; see Gheerbrant, 1995). However, the significance of this morphological affinity is unknown or uncertain. Recent studies have excluded the adapisoriculids from the crown group Placentalia, identifying them as basal eutherians (Goswami et al., 2011). In this hypothesis, the adapisoriculids are the only stem eutherians displaying dilambdodont molars. This molar morphology has actually evolved several times in placentals, especially in insectivore-like taxa (Butler, 1996). Interestingly, within the Afrotheria, it is identified as the ancestral morphotype of the Paenungulatomorpha (Gheerbrant et al., 2016). The convergence of the dilambdodont condition in the Paenungulatomorpha and the Adapisoriculidae is certainly possible or even likely. Nevertheless, most of the differences of *Hadrogeneios* from the adapisoriculids are derived features (including its much larger size). They do not a priori conflict with an ancient stem relationship of the adapisoriculids to the clade including *Hadrogeneios* (Paenungulatomorpha or Afrotheria). We should notice in passing that this is consistent with the distribution of the adapisoriculids in time (Late Cretaceous and Paleocene) and space (Africa).

Understanding the significance of the shared derived upper molar traits of *Hadrogeneios* and adapisoriculids requires additional data. We need more complete material of these taxa in order to develop further comparisons and significant formal analysis (e.g., cladistic analysis) of their relationships. Currently, the knowledge of the adapisoriculids is indeed especially poor, restricted to mostly isolated teeth (especially for African taxa!) and a few tarsal bones, making any conclusion on their relationships tentative.

Besides a basically primitive dental pattern, *Hadrogeneios phosphaticus* is characterized by a remarkable specialized anterior part of the dentary with an enlarged and stout mandibular symphysis associated to small incisors. It is interpreted as corresponding to a peculiar specialization for food acquisition with increasing grip strength or enhanced grip precision. This is the earliest specialization evidenced in the evolutionary radiation of the stem paenungulates. It is most likely an autapomorphy of *Hadrogeneios*; for instance, it is well distinctive from the more generalized condition seen in *Ocepeia* (Gheerbrant, 2010; Gheerbrant et al., 2014). However, the morphology of the mandibular symphysis, the pars incisiva, and the incisors in *Abdounodus* remain unknown, as in the ancestral morphotype of the Paenungulatomorpha. As a result, the significance of the mandibular symphyseal pattern seen in *Hadrogeneios* is still unknown in the context of the evolution of the specialized anterior dental apparatus of the crown paenungulates (e.g., the enlarged incisors).

Hadrogeneios adds to the genera *Abdounodus* and *Ocepeia* from the same Ouled Abdoun middle Paleocene phosphate levels, and it further highlights the diversity of the stem paenungulates (paenungulatomorphs). *Hadrogeneios*, *Abdounodus*, and *Ocepeia* belong to three successive stem groups that document a

basal African radiation preceding that of crown paenungulates. On the other hand, *Hadrogeneios* sheds new light on the earliest steps of the evolution of the African "ungulates" (i.e., paenungulates); it is probably rooted not far from the origin of Paenungulatomorpha based on its plesiomorphic dental morphology.

This new discovery re-emphasizes the importance of the Ouled Abdoun phosphate deposits in Morocco, which provide the earliest and best fossil evidence on the origin and early radiation of the African "ungulates".

ACKNOWLEDGMENTS

I thank N. Longrich (University of Bath) and F. Escuillié, who donated the material studied here to the collections of the Musée d'Histoire Naturelle de Marrakech (University Cadi Ayyad, Morocco) and of the Museum d'Histoire Naturelle de Toulouse (France), making it available to scientific study and publication. I thank N.E. Jalil (CR2P, MNHN), associate-researcher at University Cadi Ayyad (UCA) and curator of the MHNM-UCA collections, for making possible the study of the *Hadrogeneios* material. I thank D. Domning for kindly providing unpublished information on *Pezosiren* (Domning in press; and pers. com.). M. Bellato (MNHN) helped with the realization of the CT scans at the MNHN-AST-RX technical platform (UMS 2700, MNHN). I thank N. Poulet and F. Goussard (CR2P, 3D imaging technical platform, MNHN) for their great help with the 3D reconstruction and modelling of the material studied here, which were made from the microtomographies (Figs. 6–8; Supplementary Data 1, Figs. S2, S4). I thank C. Letenneur (CR2P, MNHN) for her talent in drawing the reconstruction of the lower jaw of *Hadrogeneios* (Fig. 9). I thank L. Cases (CR2P, CNRS) and P. Loubry (CR2P, CNRS) for the photographs (Figs. 1–

5). I thank R. Vacant (CR2P, CNRS), S. Colas (CR2P, MNHN), and Y. Despres (CR2P, MNHN) for preparation and casting of the specimens. I thank A. Lethiers (CR2P, Sorbonne Université) for his help in formatting the figures. I thank the reviewers and editors for corrections and suggestions that helped to improve the manuscript of this paper.

SUPPLEMENTARY INFORMATION

Supplementary Data 1.pdf: Tables S1-S5, Figures S1-S5.

Supplementary Data 2.pdf: Phylogenetic analysis of *Hadrogeneios phosphaticus,* gen. et sp. nov.

Supplementary Data 3.nex: Analyzed phylogenetic matrix including *Hadrogeneios phosphaticus,* gen. et sp. nov.

Supplementary Data 4–6.tre: Complete set of # most parsimonious trees obtained in the parsimony analysis.

Supplementary Data 7–9.pdf: 3D models from CT scans of MHNM.KHG.224 (paratype of *Hadrogeneios phosphaticus*), MHNM.KHG.225 (paratype of *Hadrogeneios phosphaticus*), and MHNM.KHG.227 (holotype of *Hadrogeneios phosphaticus*).

ORCID

Emmanuel Gheerbrant https://orcid.org/0000-0003-3355-458X

LITERATURE CITED

Arambourg, C. (1952). Les vertébrés fossiles des gisements de phosphates (Maroc-Algérie-Tunisie). *Notes et Mémoires du Service Géologique du Maroc*, *92*, 1–372.

Butler, P. M. (1996). Dilambdodont molars: A functional interpretation of their evolution. *Palaeovertebrata*, *25*, 205–213.

Crochet, J. Y. (1984). *Garatherium mahboubii* nov. gen., nov. sp., Marsupial de l'Eocène inférieur d'El Kohol (Sud Oranais, Algérie). *Annales de Paléontologie (Vertébrés-Invertébrés)*, *70*, 275–294.

Crompton, A. W. (1971). The origin of the tribosphenic molar. Zoolo*gical Journal of the Linnean Society*, *50*, 65–87.

Domning, D. P. (2001). The earliest known fully quadrupedal sirenian. *Nature*, *413*, 625–627.

Domning, D. P. (in press). The Sirenia (Mammalia: Prorastomidae) of the Eocene Seven Rivers site, Jamaica. In R. W. Portell, & D. P. Domning (Eds.), *The Sirenia (Mammalia: Prorastomidae) of the Eocene Seven Rivers site, Jamaica*. Springer.

Domning, D. P., Heal, G. J., & Sorbi, S. (2017). *Libysiren sickenbergi*, gen. et sp. nov.: a new sirenian (Mammalia, Protosirenidae) from the middle Eocene of Libya. Jo*urnal of Vertebrate Paleontology*, *37*,1–17.

Gheerbrant, E. 1995. Les mammifères paléocènes du Bassin d'Ouarzazate (Maroc). III. Adapisoriculidae et autres mammifères (Carnivora, ?Creodonta, Condylarthra, ?Ungulata et *incertae sedis*). *Palaeontographica* A 237:39–132.

Gheerbrant, E. 2009. Paleocene emergence of elephant relatives and the rapid radiation of African ungulates. *Proceedings of the National Academy of Sciences* 106:10717–10721.

Gheerbrant, E. 2010. Primitive African ungulates ("Condylarthra" and Paenungulata); pp. 563–571 in L. Werdelin and W. J. Sanders (eds.), *Cenozoic Mammals of Africa*. University of California Press, Berkeley, Los Angeles, London.

Gheerbrant, E., M. Amaghzaz, B. Bouya, F. Goussard, & Letenneur, C. 2014. *Ocepeia* (Middle Paleocene of Morocco): The Oldest Skull of an Afrotherian Mammal. PLoS ONE 9:e89739.

Gheerbrant, E., B. Bouya, & Amaghzaz, M. 2012. Dental and cranial anatomy of *Eritherium azzouzorum* from the Paleocene of Morocco, earliest known proboscidean mammal. *Palaeontographica* A 297:151–183.

Gheerbrant, E., A. Filippo, & Schmitt, A. 2016. Convergence of Afrotherian and Laurasiatherian Ungulate-Like Mammals: First Morphological Evidence from the Paleocene of Morocco. *PLoS ONE* 11:e89739.

Gheerbrant, E., J. Sudre, & Cappetta, H. 1996. A Palaeocene proboscidean from Morocco. *Nature* 383:68–70.

Gheerbrant, E., F. Khaldoune, A. Schmitt, & Tabuce, R. 2021. Earliest embrithopod mammals (Afrotheria, Tethytheria) from the Early Eocene of Morocco: anatomy, systematics and phylogenetic significance. *Journal of Mammalian Evolution* 28:245–283.

Gheerbrant, E., J. Sudre, M. Iarochene, & Moumni, A. 2001. First ascertained African "condylarth" mammals (primitive ungulates: cf. Bulbulodentata & cf. Phenacodonta) from the Earliest Ypresian of the Ouled Abdoun Basin, Morocco. *Journal of Vertebrate Paleontology* 21:107–118.

Gheerbrant, E., J. Sudre, H. Cappetta, C. Mourer-Chauvire, E. Bourdon, M. Iarochene, M. Amaghzaz, & Bouya, B. 2003. Les localités à mammifères des carrières de Grand Daoui, Bassin des Ouled Abdoun, Maroc, Yprésien : premier état des lieux. *Bulletin de la Société Géologique de France* 174:279–293.

Goloboff, P. A., & Catalano, S. A. 2016. TNT version 1.5, including a full implementation of phylogenetic morphometrics. *Cladistics* 32:221–238.

Goloboff, P. A., J. S. Farris, & Nixon, K. C. 2008. TNT, a free program for phylogenetic analysis. *Cladistics* 24:774–786.

Goswami, A., G. V. R. Prasad, P. Upchurch, D. Boyer, E. Seiffert, O. Verma, E. Gheerbrant, & Flynn, J. J. 2011. A radiation of arboreal basal eutherian mammals beginning in the Late Cretaceous of India. *Proceeding of the National Academy of Sciences* 108:16333–16338.

Kocsis, L., A. Ulianov, M. Mouflih, F. Khaldoune, & Gheerbrant, E. 2021. Geochemical investigation of the taphonomy, stratigraphy, and palaeoecology of the mammals from the Ouled Abdoun Basin (Paleocene-Eocene of Morocco). *Palaeogeography, Palaeoclimatology, Palaeoecology* 577:1–17.

Kocsis, L., E. Gheerbrant, M. Mouflih, H. Cappetta, J. Yans, & Amaghzaz, M. 2014. Comprehensive stable isotope investigation of marine biogenic apatite from the late Cretaceous–early Eocene phosphate series of Morocco. *Palaeogeography, Palaeoclimatology, Palaeoecology* 394:74–88.

Kocsis, L., E. Gheerbrant, M. Mouflih, H. Cappetta, A. Ulianov, M. Chiaradia, & Bardet, N. 2016. Gradual changes in upwelled seawater conditions (redox, pH) from the late Cretaceous through early Paleogene at the northwest coast

of Africa: Negative Ce anomaly trend recorded in fossil bio-apatite. *Chemical Geology* 421:44–54.

Kramarz, A. G., M. Bond, & Carlini, A. A. 2019. Astrapotheres from Cañadón Vaca, middle Eocene of central Patagonia. New insights on diversity, anatomy, and early evolution of Astrapotheria. *Palaeontologia Electronica* 22:1–22.

Matthew, W. D., & Granger, W. 1915. A revision of the Lower Eocene Wasatch and Wind River faunas. *Bulletin of the American Museum of Natural History* 34:1–103.

McClung, J. R., & Goldberg, S. J. 2000. Functional anatomy of the hypoglossal innervated muscles of the rat tongue: A model for elongation and protrusion of the mammalian tongue. *The Anatomical Record* 260:378–386.

O'Leary, M. A., J. I. Bloch, J. J. Flynn, T. J. Gaudin, A. Giallombardo, N. P. Giannini, S. L. Goldberg, B. P. Kraatz, Z.-X. Luo, J. Meng, X. Ni, M. J. Novacek, F. A. Perini, Z. S. Randall, G. W. Rougier, E. J. Sargis, M. T. Silcox, N. B. Simmons, M. Spaulding, P. M. Velazco, M. Weksler, J. R. Wible, & Cirranello, A. L. 2013. The Placental Mammal Ancestor and the Post-K-Pg Radiation of Placentals. *Science* 339:662–667.

Schultz, J. A., S. Engels, L. C. Schwermann, & Koenigswald, W. v. 2020. Evolutionary Trends in the Mastication Patterns in Some Perissodactyls, Cetartiodactyls, & Proboscideans; pp. 215–230 in T. Martin, W. von Koenigswald (eds), *Mammalian Teeth: Form and Function*. Verlag Dr. Friedrich Pfeil, Munich.

Schultz, J. A., U. Menz, D. E. Winkler, E. Schulz-Kornas, S. Engels, D. C. Kalthoff, W. von Koenigswald, I. Ruf, T. M. Kaiser, O. Kullmer, K.-H. Südekum, &

Martin, T. 2018. Modular Wear Facet Nomenclature for mammalian post-canine dentitions. *Historical Biology* 30:30–41.

Scott, C. S. 2010. New cyriacotheriid pantodonts (Mammalia, Pantodonta) from the Paleocene of Alberta, Canada, and the relationships of Cyriacotheriidae. *Journal of Paleontology* 84:197–215.

Seiffert, E. R. 2010. The Oldest and Youngest Records of Afrosoricid Placentals from the Fayum Depression of Northern Egypt. *Acta Palaeontologica Polonica* 55:599–616.

Seiffert, E. R., & Simons, E. L. 2000. *Widanelfarasia*, a diminutive placental from the Late Eocene of Egypt. *Proceedings of the National Academy of Sciences* 97:2646–2651.

Solé, F., E. Gheerbrant, M. Amaghzaz, & Bouya, B. 2009. Further evidence of the African antiquity of hyaenodontid ('Creodonta', Mammalia) evolution. *Zoological Journal of the Linnean Society* 156:827–846.

Stanhope, M. J., V. G. Waddell, O. Madsen, W. de Jong, S. B. Hedges, G. C. Cleven, D. Kao, & Springer, M. S. 1998. Molecular evidence for multiple origins of Insectivora and for a new order of endemic African insectivore mammals. *Proceedings of the National Academy of Sciences* 95:9967–9972.

Van Valen, L. V. 1966. Deltatheridia, a new order of mammals. *Bulletin of the American Museum of Natural History* 132:1–126.

Yans, J., M. Amaghzaz, B. Bouya, H. Cappetta, P. Iacumin, L. Kocsis, M. Mouflih, O. Selloum, S. Sen, J.-Y. Storme, & Gheerbrant, E. 2014. First carbon isotope chemostratigraphy of the Ouled Abdoun phosphate Basin, Morocco; implications for dating and evolution of earliest African placental mammals. *Gondwana Research* 25:257–269.

Submitted July 9, 2022; revision received January 17, 202r; accepted MONTH DD, YYYY.

Handling Editor: NNNN.

CAPTION OF FIGURES

FIGURE 1. *Hadrogeneios phosphaticus*, gen. et sp. nov., MHNM.KHG.226. **A**, right M2–3; **B**, associated left M3 of the same individual. **C**. MHNM.KHG.223, right M3. Occlusal views, s.e.m. photographs. [column width]

FIGURE 2. *Hadrogeneios phosphaticus*, gen. et sp. nov. ~~Holotype MHNM.KHG.227, part of left dentary preserving the mandibular symphysis, the alveoli for two incisors, c1 and p1–3 and p4, m1 and m3 that is broken apart. **A–C**, occlusal (stereophotographic views), labial and lingual views of the dentary. **D–F**, details of p4–m1 in occlusal (stereophotographic views), labial and lingual views; **G–E**, the isolated m3, broken from the dentary, in occlusal (stereophotographic views), labial and lingual views.~~ [page width]

FIGURE 3. *Hadrogeneios phosphaticus*, gen. et sp. nov. ~~**A–C,** MHNM.KHG.224, part of right dentary broken in several pieces in occlusal (stereophotographic views), lingual and labial views; it preserves the mandibular symphysis, p3–4, m2, and the alveoli for i1–3, c1, and p1. **D–F**, MHNM.KHG.225, posterior part of a left dentary with m2 and m3, in occlusal (stereophotographic views), lingual and labial views. **G–J,** MHNT PAL 2006.0.19, broken posterior part of right dentary with m3 in occlusal~~

view (G: stereophotographic views; J: enlarged view) and lingual and labial views.

[page width]

FIGURE 4. *Hadrogeneios phosphaticus*, gen. et sp. nov. Detailed occlusal view of the lower teeth (s.e.m. photographs). **A**. Holotype MHNM.KHG.227, left p4, m1 and m3. **B**. MHNM.KHG.224, right p3–4, and m2. **C**. MHNM.KHG.225, left m2 and m3. **D**. MHNT PAL 2006.0.19, right m3. [page width]

FIGURE 5. *Hadrogeneios phosphaticus*, gen. et sp. nov. Composite reconstruction of the lower cheek-tooth row, occlusal sketches. **A**, p3–4: MHNM.KHG.224 in reversed view; M1: MHNM.KHG.227; m2: MHNM.KHG.224; m3: MHNT PAL 2006.0.19 in reversed view; alveoli of p4 and p3 from MHNM.KHG.224. **B**, p3–4: MHNM.KHG.224 in reversed view; m1: MHNM.KHG.227; m2: MHNM.KHG.225; m3: MHNM.KHG.225; alveoli of p4 and p3 from MHNM.KHG.224. **C**, p4-m1: MHNM.KHG.227; m2: MHNM.KHG.225; m3: MHNM.KHG.227; alveoli of p4, dp3 (annotated “dp”) and p3 from MHNM.KHG.227. [column width]

FIGURE 6. *Hadrogeneios phosphaticus*, gen. et sp. nov. Composite reconstructions of the lower tooth row based on the 3D digital models made from the CT scans of the material. **A,** Occlusal sketch of the left lower tooth row: alveoli of i1–3, c1 and p1–2, and the teeth p3–4; m1–3. **B**–**C**, 3D digital models in occlusal and lingual views. **B**, alveoli of i1–3, c1, and p1–2, and the teeth p3–4 and m1–3. **C**, alveoli of i1–3, c, p1–3 (dp3 in grey), and p4, m1–3. The specimen numbers for the 3D digital models are indicated below the teeth. [2/3 page width]

FIGURE 7. *Hadrogeneios phosphaticus*, gen. et sp. nov. 3D digital models of lower jaws. **A**, holotype MHNM.KHG.227 in labial and lingual views. **B**, same views by transparency of the holotype MHNM.KHG.227, showing mandibular endostructures such as tooth roots, tooth alveoli, mandibular canal and efferent dorsal canaliculi. **C**,

holotype MHNM.KHG.227 in occlusal view. **D**, MHNM.KHG.224 in labial and lingual views. **E**, same views by transparency of MHNM.KHG.224 showing the mandibular endostructures. **F**, MHNM.KHG.224 in occlusal view. Note the remarkable thin and long neurovascular canaliculi that feeds the incisors, which are in a high position at the top of the symphyseal region. **Abbreviations**: **al**, tooth alveolus; **can**, dorsal canaliculi; **mc**, mandibular canal; **mf**, mental foramen; **symp**, mandibular symphysis. [page width]

FIGURE 8. *Hadrogeneios phosphaticus*, gen. et sp. nov. 3D digital model of the mandibular endostructures of MHNM.KHG.224. **A**–**B**, detail of the morphology and relationships of the mandibular canal, dorsal canaliculi, and teeth or tooth alveoli; lingual and labial views. **C**, occlusal view of the dentary. **D**–**E**, detail of the morphology of the mandibular canal and the efferent dorsal canaliculi of the incisors in dorsal and anterior views. Note that the dorsal canaliculus of i3 is very long, detaching more posteriorly than those of I2 and I1 that separates anteriorly and at a high level in the symphyseal region. **Abbreviations**: **al**, tooth alveolus; **can**, dorsal canaliculi; **mand can**, mandibular canal; **ment for**, mental foramen. [2/3 page width]

FIGURE 9. *Hadrogeneios phosphaticus*, gen. et sp. nov. Composite reconstruction of the mandible, based on the assemblage of the 3D digital models of the specimens MHNM.KHG.224 (a), MHNM.KHG.227 (b, holotype), and MHNM.KHG.225 (c); all specimens were assembled and adjusted to the size of MHNM.KHG.224. **A**. lingual view. **B**. Labial view. **C**. Sketch showing the associated and reconstructed parts in the composite reconstruction. Drawing by C. Letenneur. [2/3 page width]

FIGURE 10. Phylogenetic relationships of *Hadrogeneios phosphaticus*, gen. et sp. nov. Strict consensus of 180 MPTs from unweighted and unconstrained standard analysis with TNT 1.5 and with ordered characters. Relative Bremer index >1 (out of

10) is indicated below the nodes. Tree Length (L)= 972 steps; Retention Index (RI)= 61.3; Consistency Index (CI)= 34.8. Synapomorphies at the node Paenungulatomorpha including *Hadrogeneios*: 38–1, 55–1, 62–1, 104–1, 113–2. See Supplementary Data 2 for additional details.

[column width]

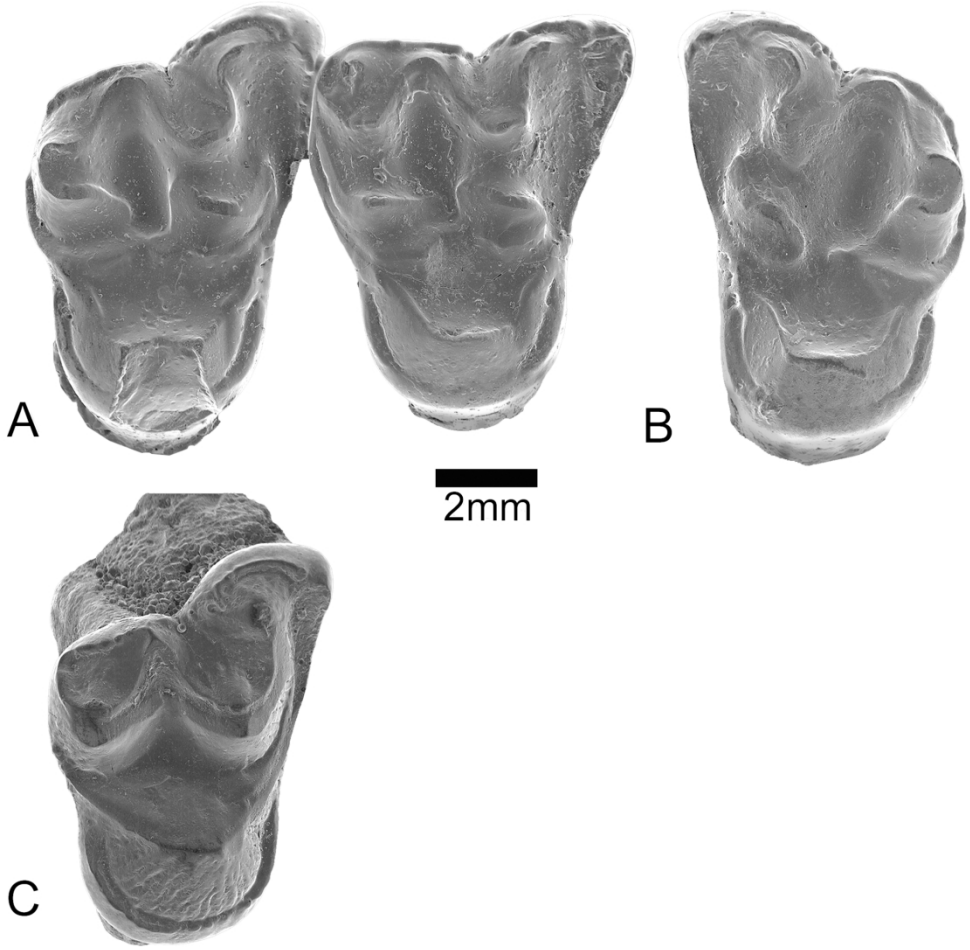

Caption : FIGURE 1. Hadrogeneios phosphaticus n. g., n. sp., MHNM.KHG.226. A, right M2-3; B, associated left M3 of the same individual. C. MHNM.KHG.223, right M3. Occlusal views, s.e.m. photographs.

90x89mm (600 x 600 DPI)

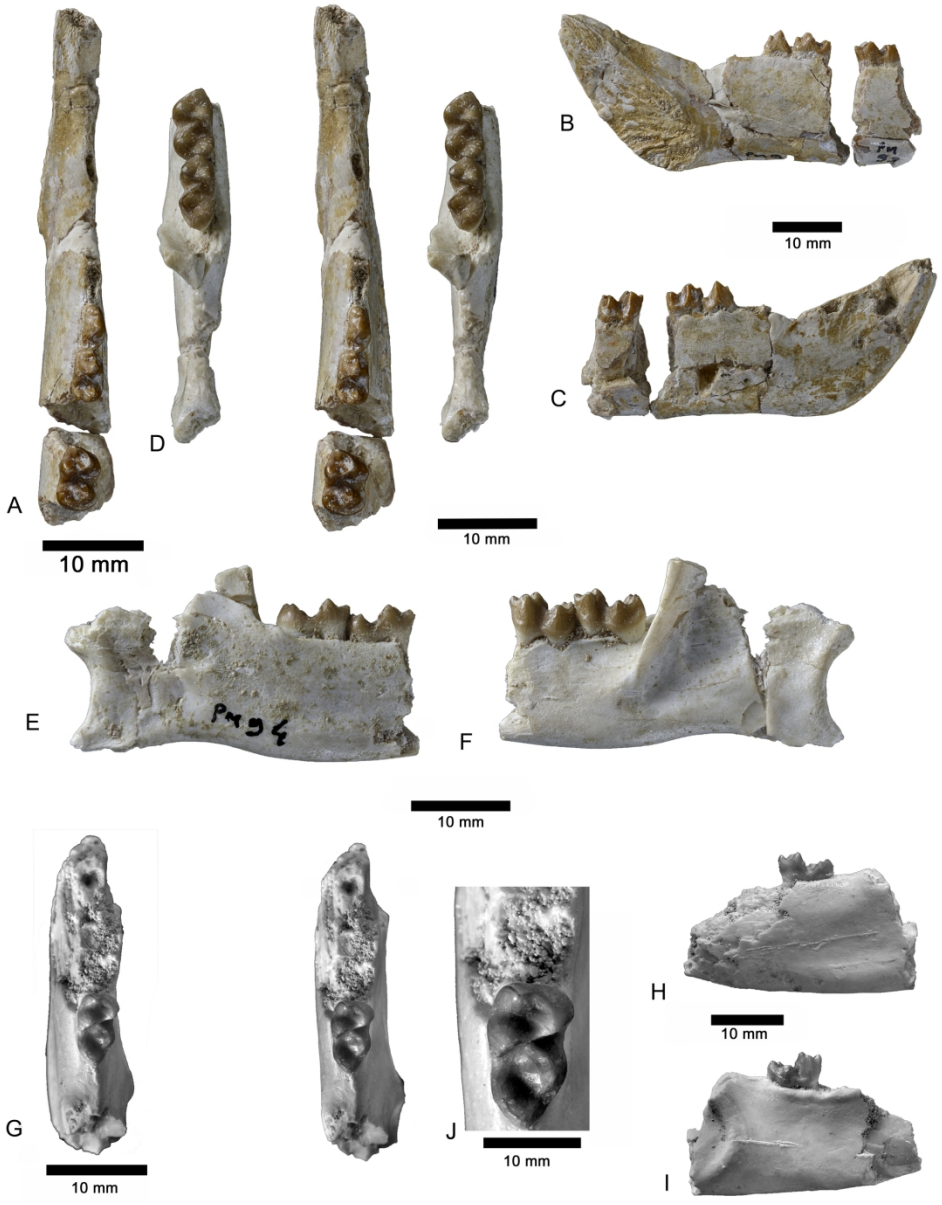

FIGURE 2 (color). Hadrogeneios phosphaticus n. g., n. sp. ~~Holotype MHNM.KHG.227, part of left dentary preserving the mandibular symphysis, the alveoli for two incisors, c1 and p1-3 and p4, m1 and m3 that is broken apart. A-C, occlusal (stereophotographic views), labial and lingual views of the dentary. D-F, details of p4-m1 in occlusal (stereophotographic views), labial and lingual views; G-E, the isolated m3, broken from the dentary, in occlusal (stereoviews), labial and lingual views.~~ Scales in millimeters.

182x227mm (300 x 300 DPI)

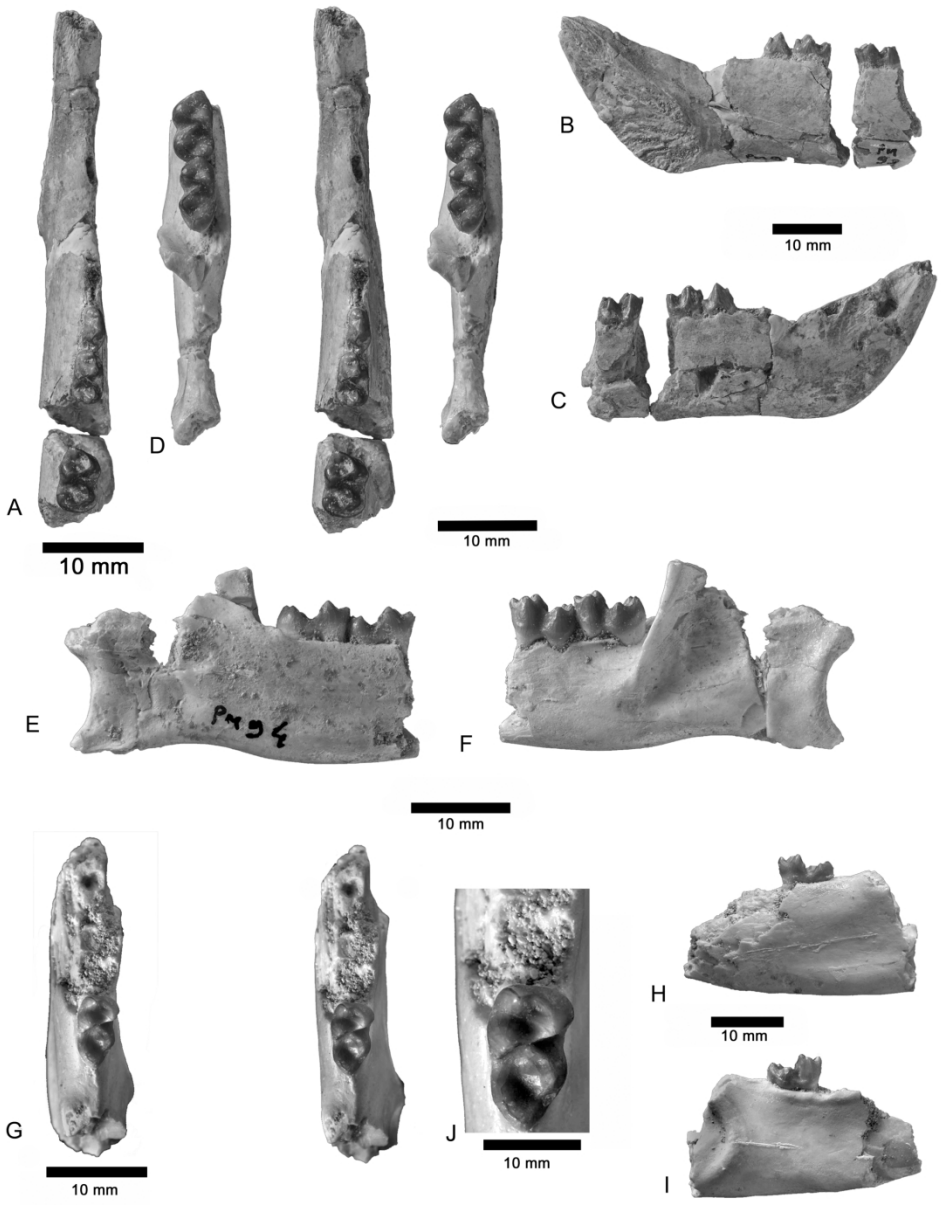

FIGURE 2 (greyscale). Hadrogeneios phosphaticus n. g., n. sp. ~~Holotype MHNM.KHG.227, part of left dentary preserving the mandibular symphysis, the alveoli for two incisors, c1 and p1-3 and p4, m1 and m3 that is broken apart. A-C, occlusal (stereophotographic views), labial and lingual views of the dentary. D-F, details of p4-m1 in occlusal (stereophotographic views), labial and lingual views; G-E, the isolated m3, broken from the dentary, in occlusal (stereoviews), labial and lingual views. Scales in millimeters.~~

182x227mm (300 x 300 DPI)

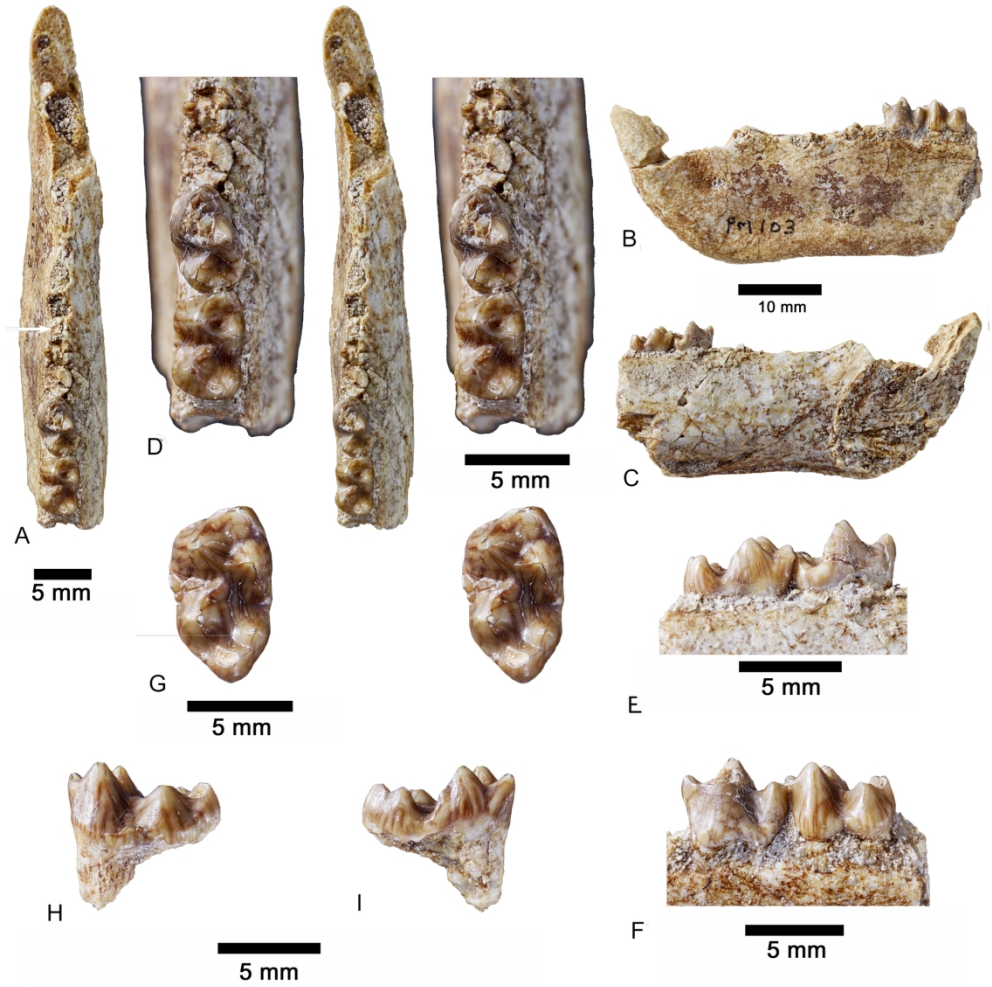

FIGURE 3 (color). Hadrogeneios phosphaticus n. g., n. sp. ~~A-C, MHNM.KHG.224, part of right dentary broken in several pieces in occlusal (stereophotographic views), lingual and labial views; it preserves the mandibular symphysis, p3-4, m2, and the alveoli for i1-3, c1, and p1. D-F, MHNM.KHG.225, posterior part of a left dentary with m2 and m3, in occlusal (stereophotographic views), lingual and labial views. G-J, MHNT PAL 2006.0.19, broken posterior part of right dentary with m3 in occlusal view (G: stereophotographic views; J: enlarged view) and lingual and labial views.~~ Scales in millimeters.

182x190mm (300 x 300 DPI)

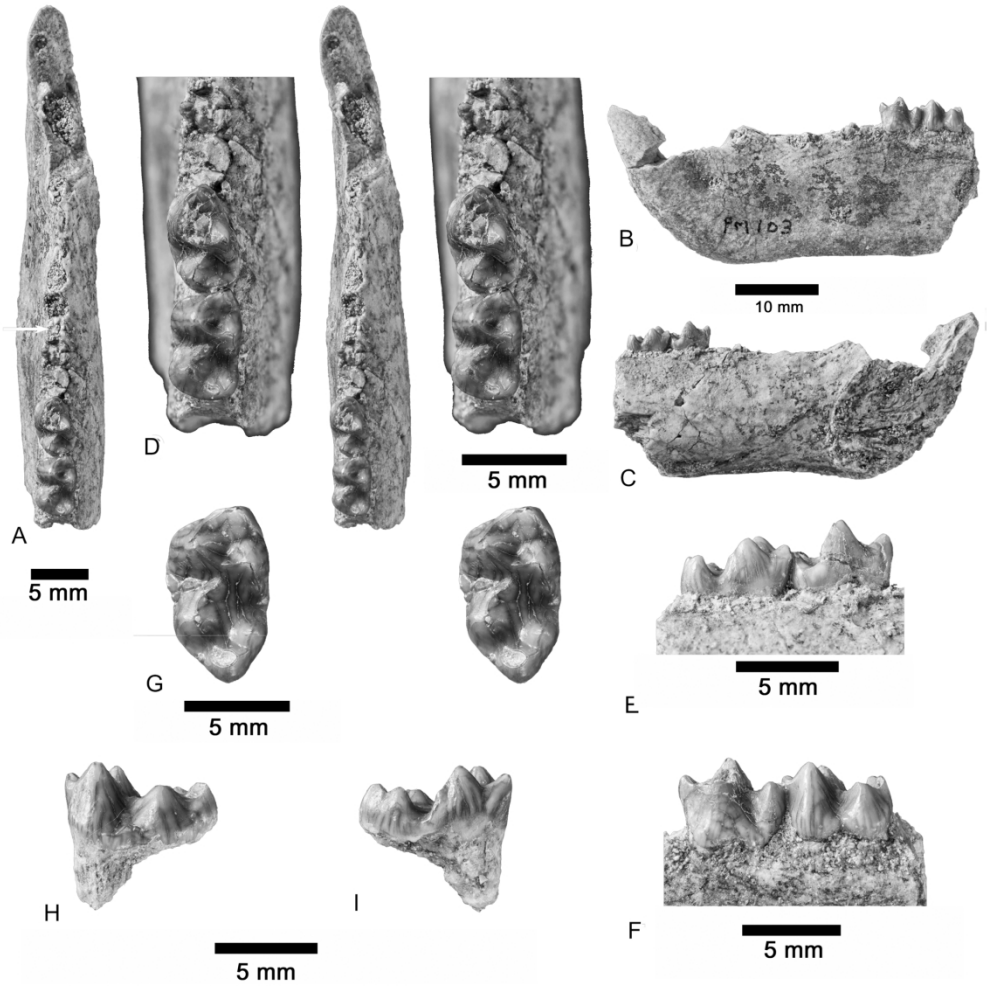

FIGURE 3 (greyscale). Hadrogeneios phosphaticus n. g., n. sp. A-C, MHNM.KHG.224, part of right dentary broken in several pieces in occlusal (stereophotographic views), lingual and labial views; it preserves the mandibular symphysis, p3-4, m2, and the alveoli for i1-3, c1, and p1. D-F, MHNM.KHG.225, posterior part of a left dentary with m2 and m3, in occlusal (stereophotographic views), lingual and labial views. G-J, MHNT PAL 2006.0.19, broken posterior part of right dentary with m3 in occlusal view (G: stereophotographic views; J: enlarged view) and lingual and labial views. Scales in millimeters.

182x190mm (300 x 300 DPI)

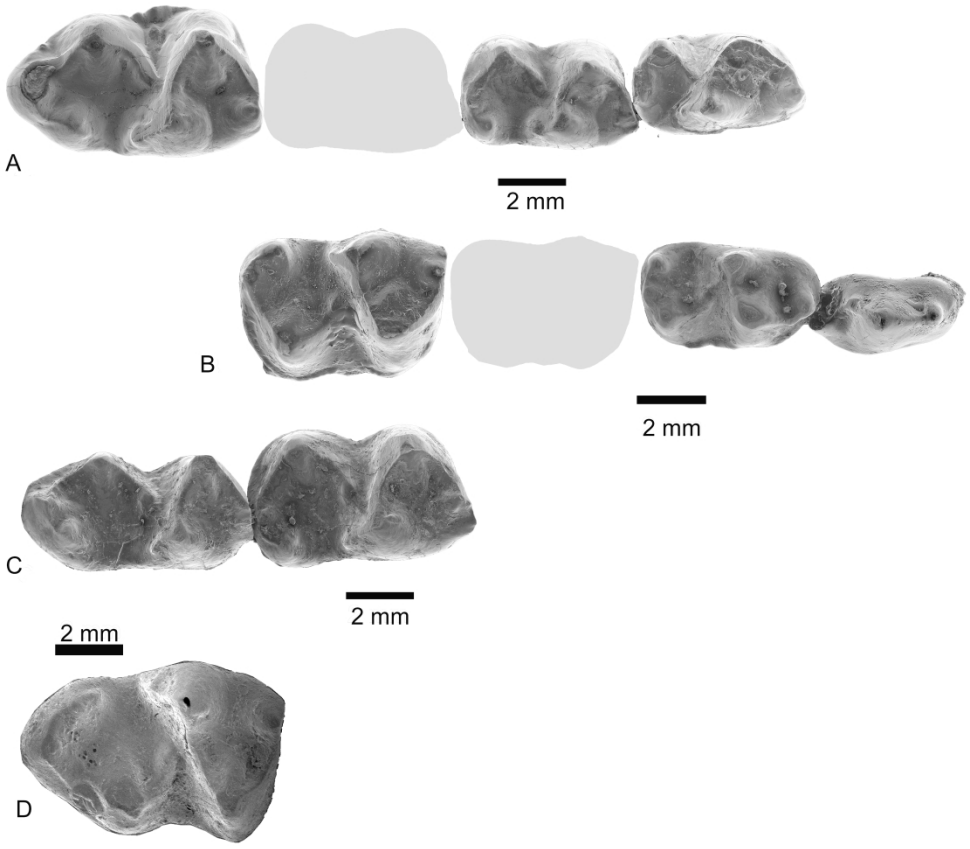

FIGURE 4. Hadrogeneios phosphaticus gen. et sp. nov. Detailed occlusal view of the lower teeth (s.e.m. photographs). A. Holotype MHNM.KHG.227, left p4, m1 and m3. B. MHNM.KHG.224, right p3–4, and m2. C. MHNM.KHG.225, left m2 and m3. D. MHNT PAL 2006.0.19, right m3.

180x161mm (600 x 600 DPI)

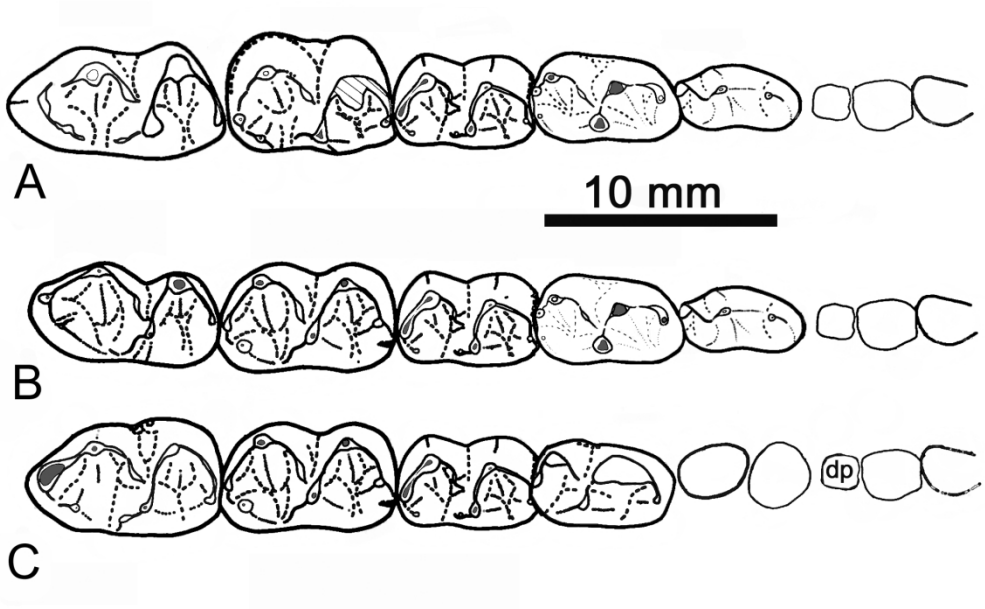

FIGURE 5. Hadrogeneios phosphaticus gen. et sp. nov. Composite reconstruction of the lower cheek-tooth row, occlusal sketches. A, p3–4: MHNM.KHG.224 in reversed view; M1: MHNM.KHG.227; m2: MHNM.KHG.224; m3: MHNT PAL 2006.0.19 in reversed view; alveoli of p4 and p3 from MHNM.KHG.224. B, p3–4: MHNM.KHG.224 in reversed view; m1: MHNM.KHG.227; m2: MHNM.KHG.225; m3: MHNM.KHG.225; alveoli of p4 and p3 from MHNM.KHG.224. C, p4-m1: MHNM.KHG.227; m2: MHNM.KHG.225; m3: MHNM.KHG.227; alveoli of p4, dp3 (annotated "dp") and p3 from MHNM.KHG.227.

88x60mm (600 x 600 DPI)

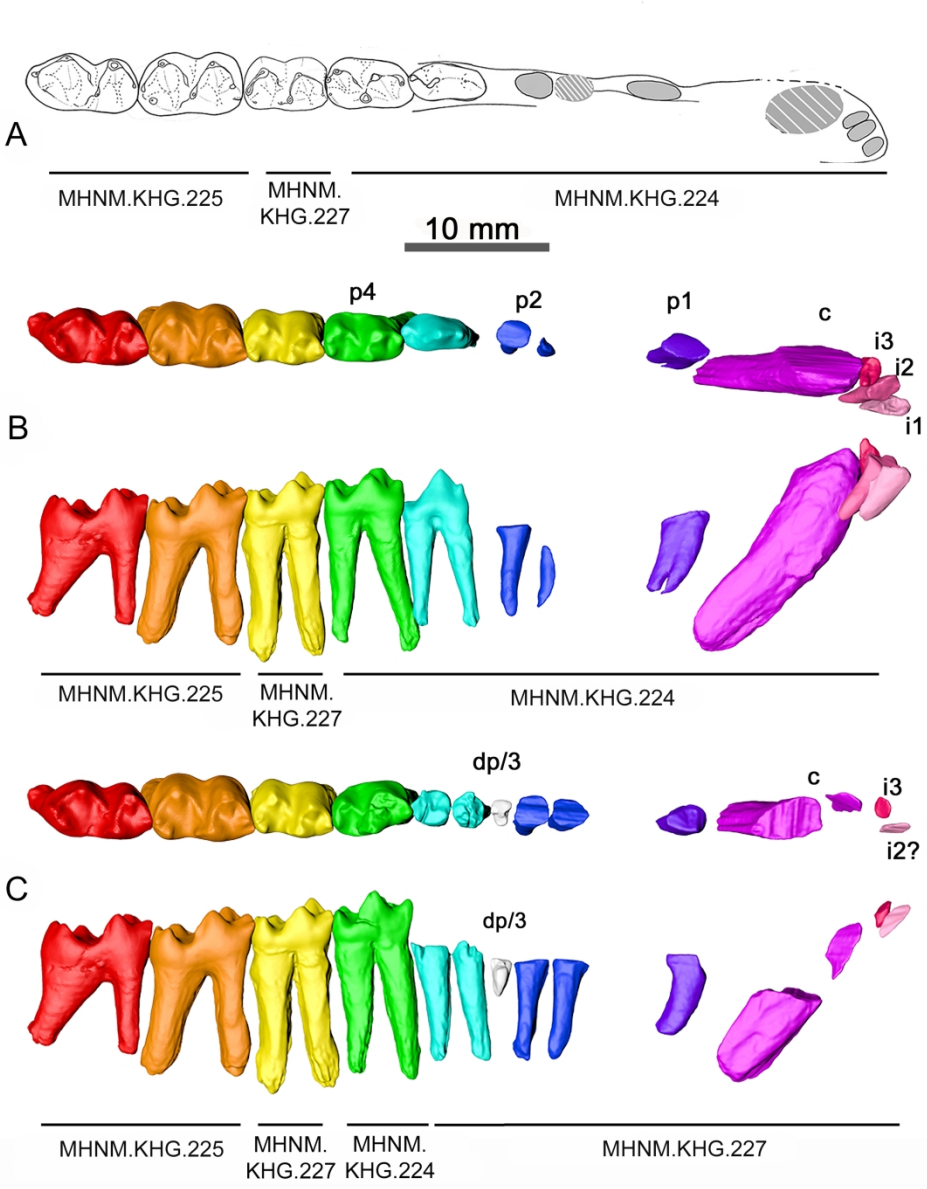

FIGURE 6 (color). Hadrogeneios phosphaticus gen. et sp. nov. Composite reconstructions of the lower tooth row based on the 3D digital models made from the CT scans of the material. A, Occlusal sketch of the left lower tooth row: alveoli of i1–3, c1 and p1–2, and the teeth p3–4; m1–3. B-C, 3D digital models in occlusal and lingual views. B, alveoli of i1–3, c1, and p1–2, and the teeth p3–4 and m1–3. C, alveoli of i1–3, c, p1–3 (dp3 in grey), and p4, m1–3. The specimen numbers for the 3D digital models are indicated below the teeth.

120x153mm (600 x 600 DPI)

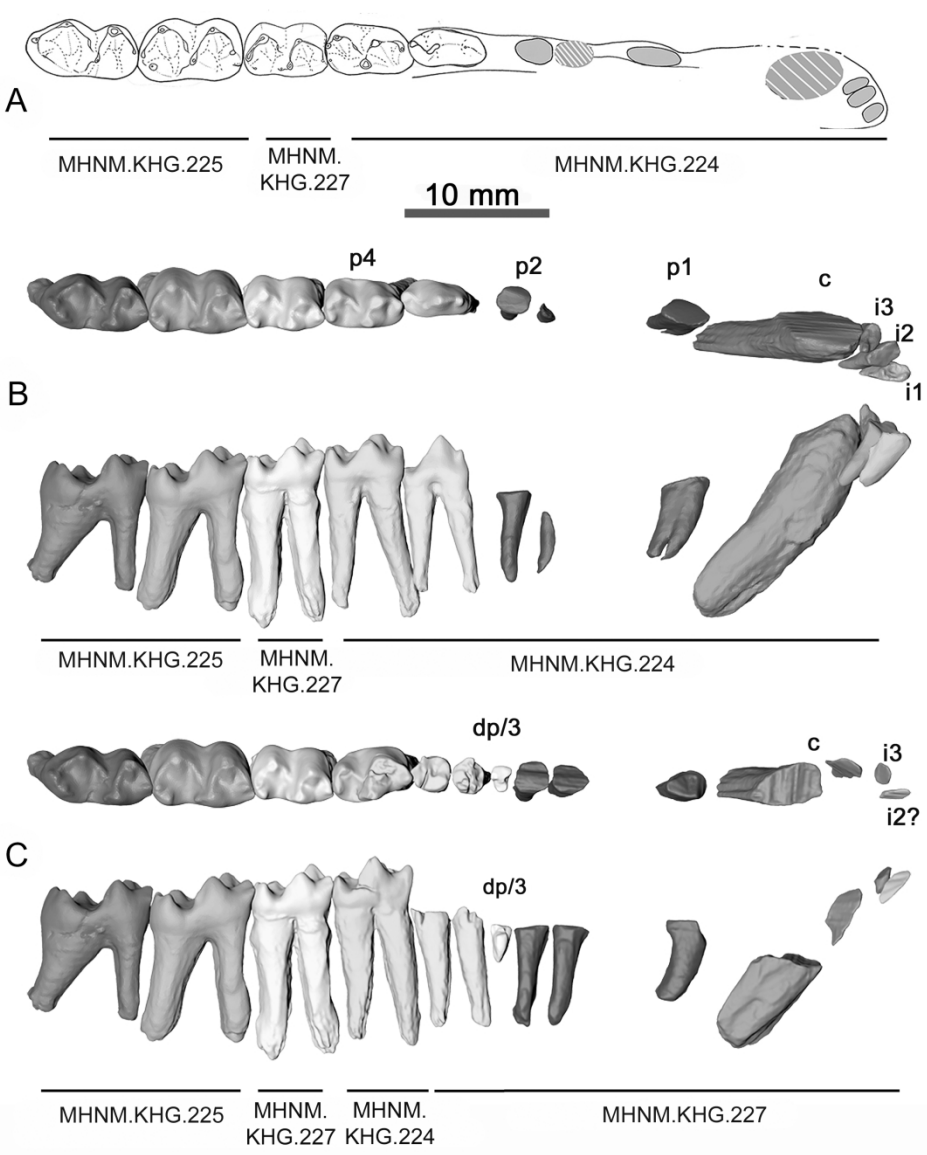

FIGURE 6 (greyscale). Hadrogeneios phosphaticus gen. et sp. nov. Composite reconstructions of the lower tooth row based on the 3D digital models made from the CT scans of the material. A, Occlusal sketch of the left lower tooth row: alveoli of i1–3, c1 and p1–2, and the teeth p3–4; m1–3. B-C, 3D digital models in occlusal and lingual views. B, alveoli of i1–3, c1, and p1–2, and the teeth p3–4 and m1–3. C, alveoli of i1–3, c, p1–3 (dp3 in grey), and p4, m1–3. The specimen numbers for the 3D digital models are indicated below the teeth.

120x153mm (600 x 600 DPI)

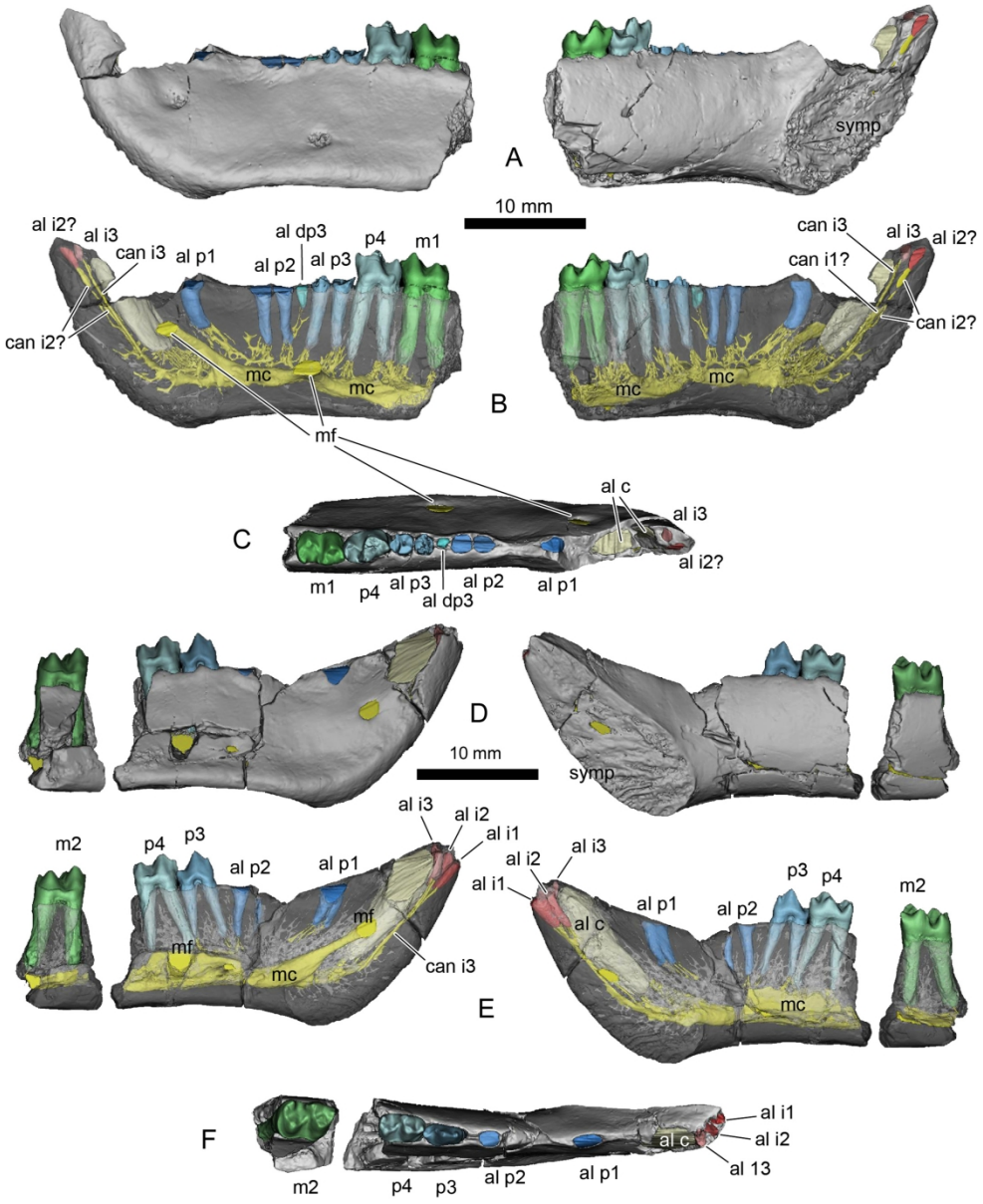

FIGURE 7 (color). Hadrogeneios phosphaticus gen. et sp. nov. 3D digital models of lower jaws. A, holotype MHNM.KHG.227 in labial and lingual view. B, same views by transparency of the holotype MHNM.KHG.227, showing mandibular endostructures such as tooth roots, tooth alveoli, mandibular canal and efferent dorsal canaliculi. C, holotype MHNM.KHG.227 in occlusal view. D, MHNM.KHG.224 in labial and lingual views. E, same views by transparency of MHNM.KHG.224 showing the mandibular endostructures. F, MHNM.KHG.224 in occlusal view. Note the remarkable thin and long neurovascular canaliculi that feeds the incisors which are in high position at the top of the symphyseal region. Abbreviations: al: tooth alveolus; can: dorsal canaliculi; mc: mandibular canal; mf: mental foramen; symp: mandibular symphysis.

183x224mm (600 x 600 DPI)

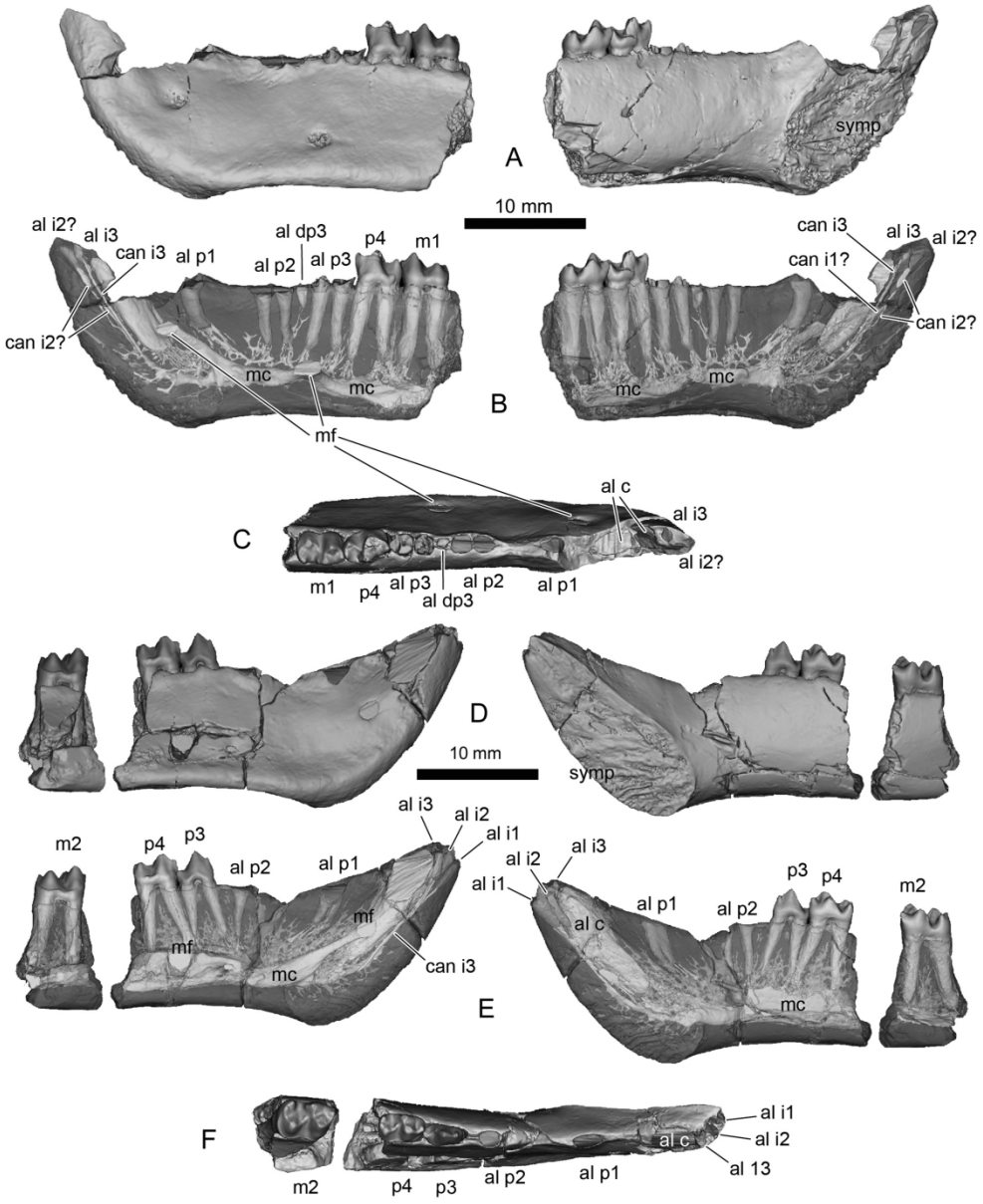

FIGURE 7 (greyscale). Hadrogeneios phosphaticus gen. et sp. nov. 3D digital models of lower jaws. A, holotype MHNM.KHG.227 in labial and lingual view. B, same views by transparency of the holotype MHNM.KHG.227, showing mandibular endostructures such as tooth roots, tooth alveoli, mandibular canal and efferent dorsal canaliculi. C, holotype MHNM.KHG.227 in occlusal view. D, MHNM.KHG.224 in labial and lingual views. E, same views by transparency of MHNM.KHG.224 showing the mandibular endostructures. F, MHNM.KHG.224 in occlusal view. Note the remarkable thin and long neurovascular canaliculi that feeds the incisors which are in high position at the top of the symphyseal region. Abbreviations: al: tooth alveolus; can: dorsal canaliculi; mc: mandibular canal; mf: mental foramen; symp: mandibular symphysis.

183x224mm (600 x 600 DPI)

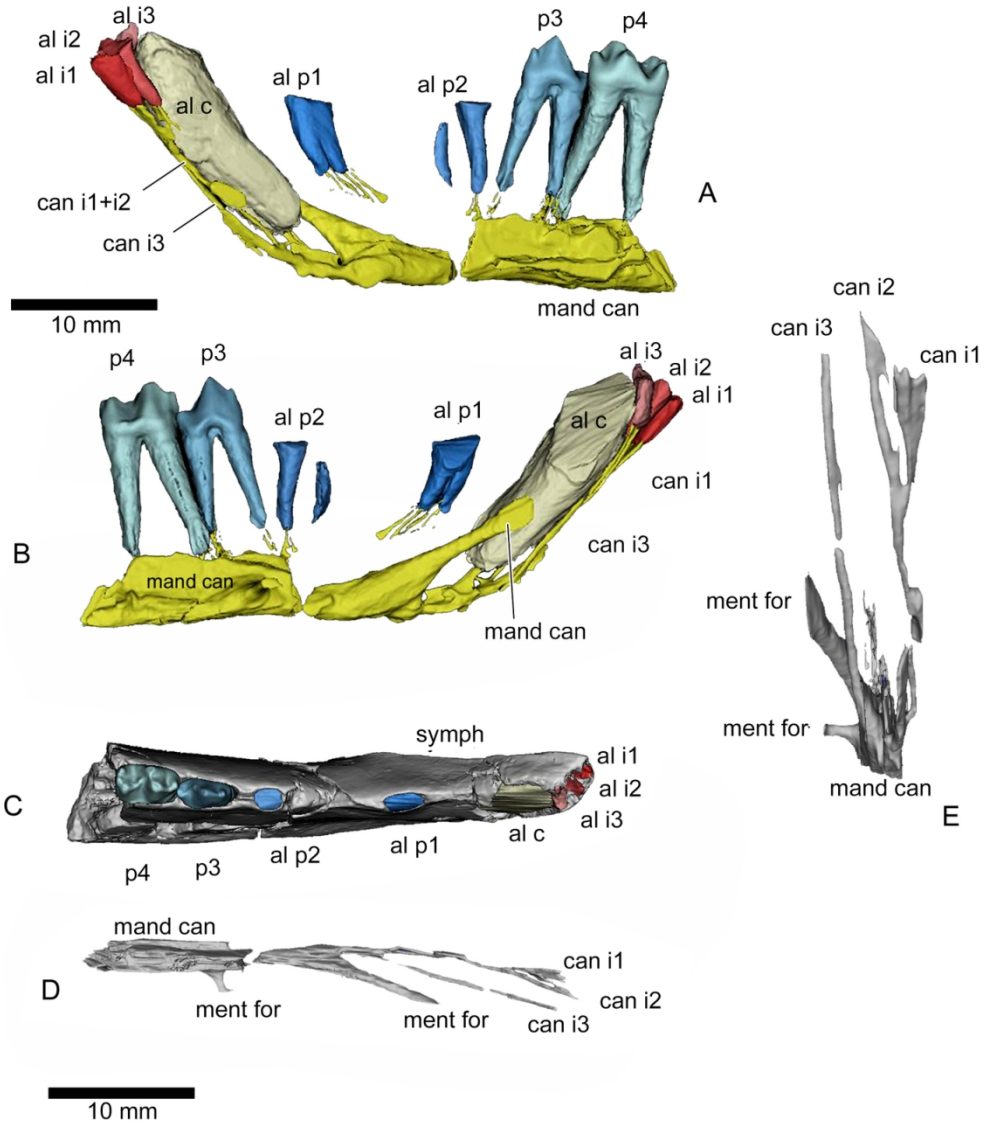

FIGURE 8 (color). Hadrogeneios phosphaticus gen. et sp. nov. 3D digital model of the mandibular endostructures of MHNM.KHG.224. A-B, Detail of the morphology and relationships of the mandibular canal, dorsal canaliculi and teeth or tooth alveoli; lingual and labial views. C, occlusal view of the dentary. D-E, detail of the morphology of the mandibular canal and the efferent dorsal canaliculi of the incisors in dorsal and anterior views. Note that the dorsal canaliculus of i3 is very long, detaching more posteriorly than those of I2 and I1 that separates anteriorly and at high level in the symphyseal region. Abbreviations: al: tooth alveolus; can: dorsal canaliculi; mand can: mandibular canal; ment for: mental foramen.

Link text : Fig. 8

120x136mm (300 x 300 DPI)

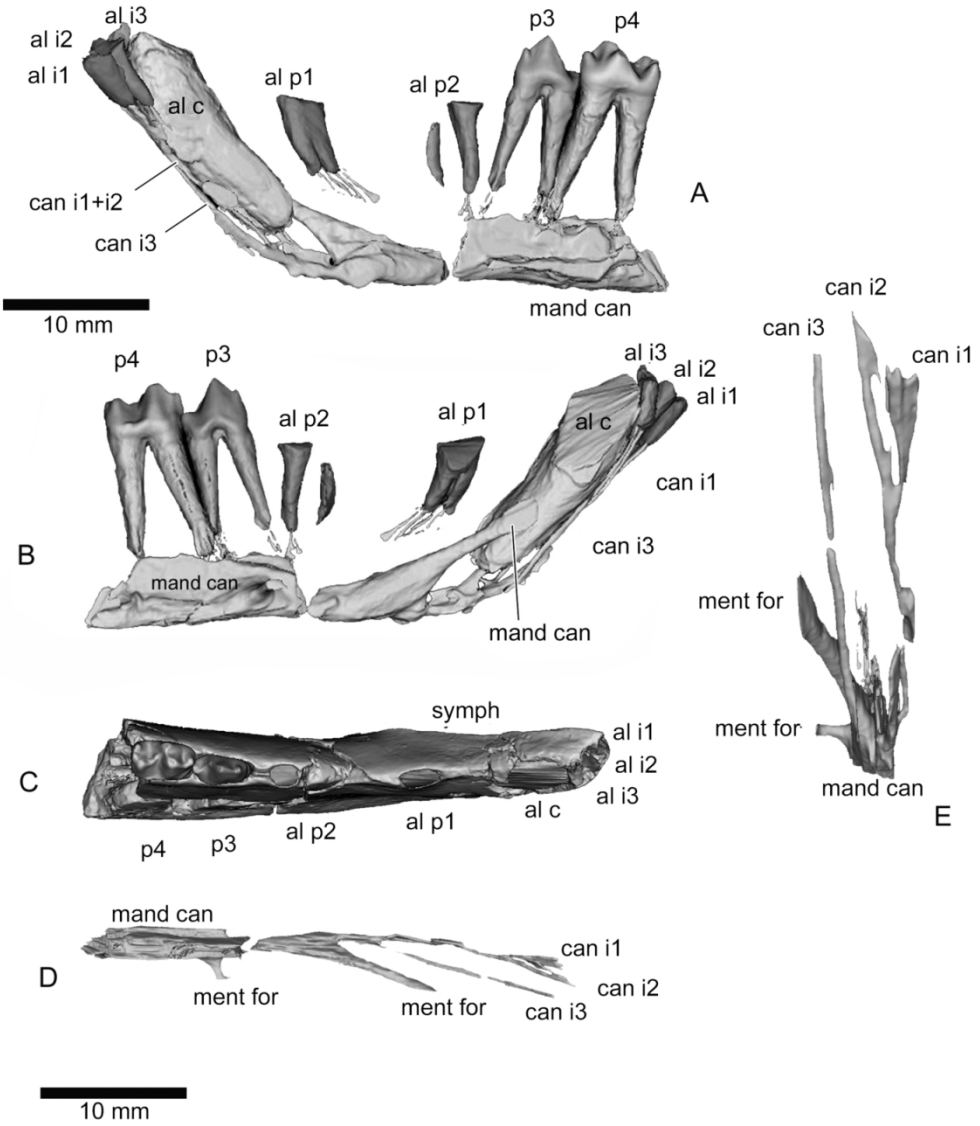

FIGURE 8 (greyscale). Hadrogeneios phosphaticus gen. et sp. nov. 3D digital model of the mandibular endostructures of MHNM.KHG.224. A-B, Detail of the morphology and relationships of the mandibular canal, dorsal canaliculi and teeth or tooth alveoli; lingual and labial views. C, occlusal view of the dentary. D-E, detail of the morphology of the mandibular canal and the efferent dorsal canaliculi of the incisors in dorsal and anterior views. Note that the dorsal canaliculus of i3 is very long, detaching more posteriorly than those of I2 and I1 that separates anteriorly and at high level in the symphyseal region. Abbreviations: al: tooth alveolus; can: dorsal canaliculi; mand can: mandibular canal; ment for: mental foramen.

120x136mm (300 x 300 DPI)

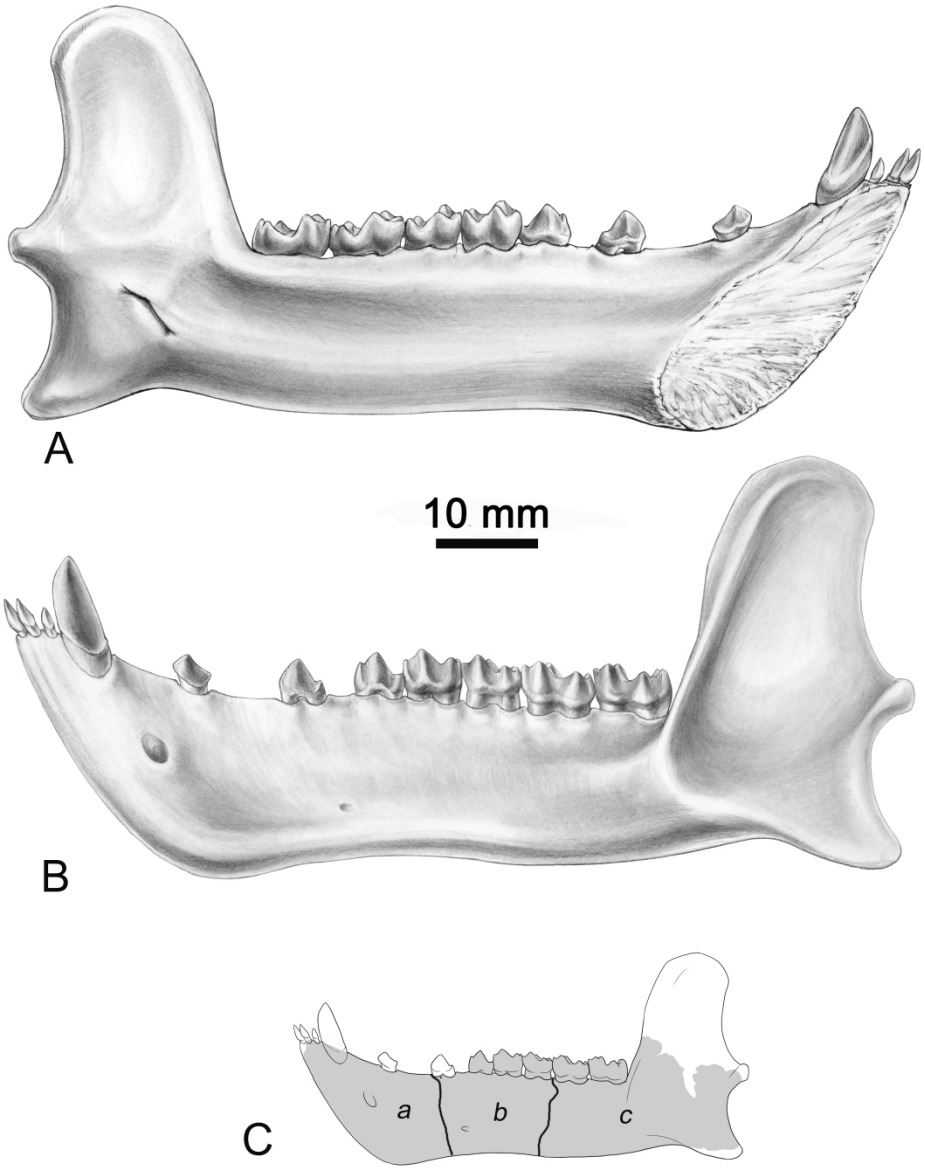

FIGURE 9. Hadrogeneios phosphaticus gen. et sp. nov. Composite reconstruction of the mandible, based on the assemblage of the 3D digital models of the specimens MHNM.KHG.224 (a), MHNM.KHG.227 (b, holotype), and MHNM.KHG.225 (c); all specimens were assembled and adjusted to the size of MHNM.KHG.224. A. lingual view. B. Labial view. C. Sketch showing the associated and reconstructed parts in the composite reconstruction. Drawing by C. Letenneur.

228x292mm (600 x 600 DPI)

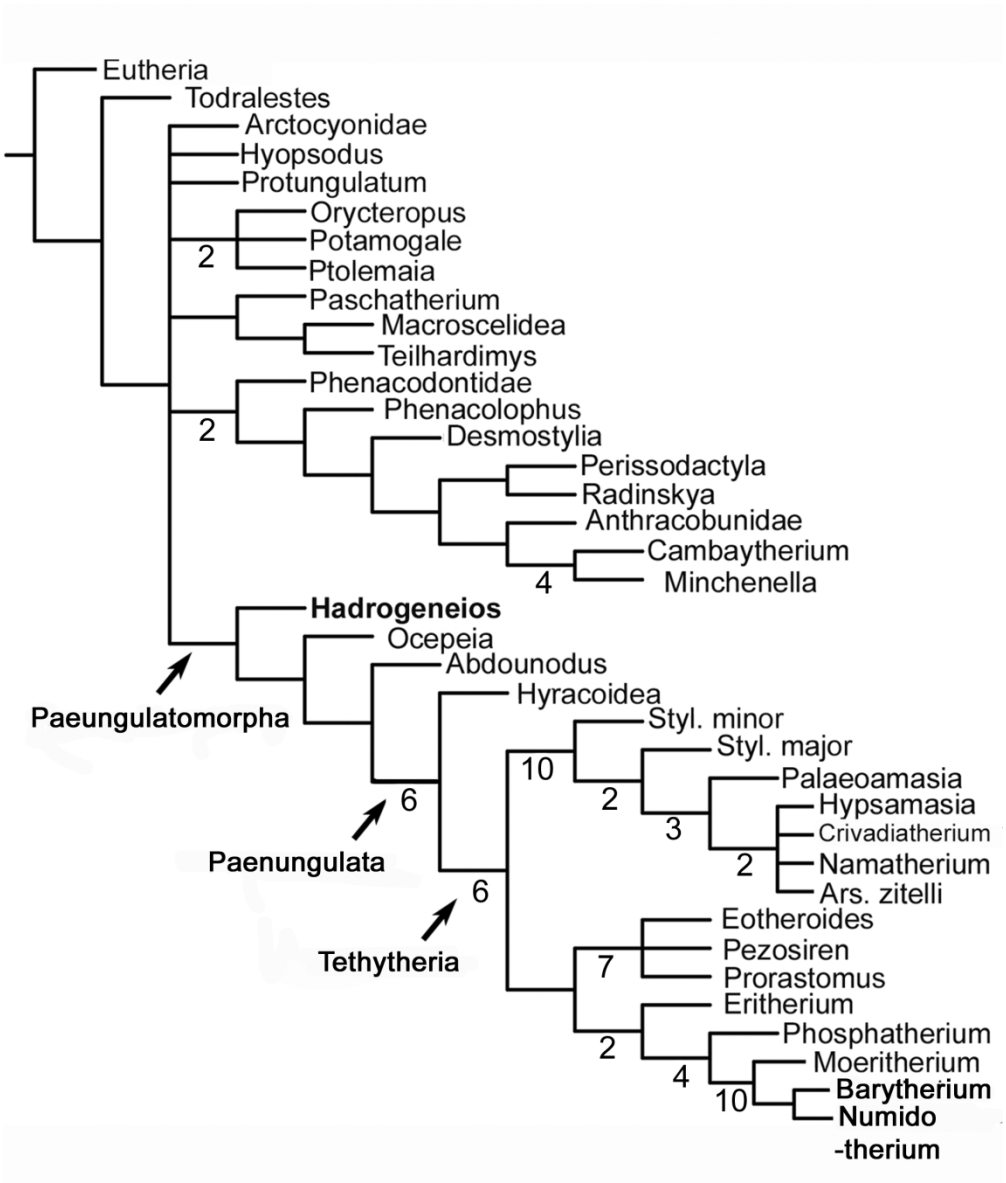

FIGURE 10. Phylogenetic relationships of Hadrogeneios phosphaticus gen. et sp. nov. Strict consensus of 130 MPTs from standard analysis with TNT 1.5 and with ordered features. Relative Bremer index >1 (out of 10) is indicated below the nodes. Tree Length (L)= 976 steps; Retention Index (RI)= 61.3; Consistency Index (CI)= 34.9. Synapomorphies at the node Paenungulatomorpha including Hadrogeneios: 38–1, 55–1, 62–1, 104–1, 113–2.

90x105mm (600 x 600 DPI)

Journal of Vertebrate Paleontology

Supplementary data

Tables S1-S5, Figures S1-S5

Ancestral radiation of paenungulate mammals (Paenungulatomorpha) - new evidence from the Paleocene of Morocco

EMMANUEL GHEERBRANT

CNRS, CR2P (CNRS-MNHN-Sorbonne Université), Museum national d'Histoire naturelle, CP38, 57 rue Cuvier, F-75231 Paris cedex 05, France, emmanuel.gheerbrant@mnhn.fr

Supplementary Tables S1-5

TABLE S1. Scan parameters of the studied material.

Specimen	Voltage	Current	Filter	Exposure	Voxel size (mm)
MHNM.KHG.225	130 kV	210 µA	0.4 mm Cu	1 s	0.02733382
MHNM.KHG.226	130 kV	210 µA	0.4 mm Cu	1 s	0.02733382
MHNM.KHG.224	140 kV	270 µA	0.5 mm Cu	1 s	0.03821419
MHNM.KHG.227	140 kV	270 µA	0.5 mm Cu	1 s	0.03821419

TABLE S2. Measurements (in mm) of upper teeth of *Hadrogeneios phosphaticus* gen. et sp. nov. Abbreviations: L, length; W, width.

Specimen	M1 L	M1 W	M2 L	M2 W	M3 L	M3 W
MHNM.KHG.223	?	?	?	?	5. 4	7. 58
MHNM.KHG.226 R	?	?	6. 5	7. 6	6. 1	8. 3
MHNM.KHG.226 L	?	?	?	?	5. 86	8. 3

TABLE S3. Length of tooth row (in mm) of *Hadrogeneios phosphaticus* gen. et sp. nov. Abbreviations: L, length; al, alveolus. *Estimated measurement.

Specimen	MHNM.KHG.225	MHNM.KHG.227	MHNM.KHG.224
L I1 (al)-M1	?	43. 35	?
L C (al)-M1	?	36. 8	?
L P1 (al)-M1	?	29. 3	?
L P2 (al)-M1	?	21. 76	?

L P3 (al)-M1	?	14. 9	?
L P4-P1 (al)	?	25. 6	?
L P3-4	?	?	9. 77
L M2-3	13. 3	?	?
Diastema C-P1	?	3.44	*4. 8
Diastema P1-2	?	4. 9	4. 5
Diastema P2-3	?	2.13	2. 13

TABLE S4. Measurements (in mm) of lower teeth of *Hadrogeneios phosphaticus* gen. et sp. nov. Abbreviations: L, length; W, width, Meas, measurements. *Estimated measurement.

Locus	Meas.	MHNT PAL 2006.0.19	MHNM. KHG.224	MHNM. KHG.225	MHNM. KHG.227
I1	L	?	*1. 1	?	?
I1	W	?	*2	?	?
I2	L	?	*1. 2	?	?
I2	W	?	*2. 4	?	?
I3	L	?	*1	?	*1
I3	W	?	*1. 4	?	*1
C	L	?	?	?	*4. 1
C	W	?	?	?	*2. 9
P1	L	?	3. 27	?	2. 8
P1	W	?	1. 5	?	1. 64
P2	L	?	*4. 7	?	4. 5
P2	W	?	*1. 53	?	2
P3	L	?	4. 16	?	*4. 9 (al)
P3	W	?	2. 35	?	*2. 5 (al)
P4	L	?	5. 44	?	5. 16
P4	W	?	3. 23	?	3. 28
M1	L	?	?	?	5. 16
M1	W	?	?	?	3. 75
M2	L	?	6. 13	6. 45	?
M2	W	?	4. 24	4. 23	?
M3	L	7.6	?	6. 85	7. 25

M3	W	4.36	?	3. 63	4. 3

TABLE S5. Measurements (in mm) of the dentary of *Hadrogeneios phosphaticus* gen. et sp. nov. *Estimated measurement.

	MHNM.KHG.224	MHNM.KHG.225	MHNM.KHG.227	MHNT PAL 2006.0.19
Max. Length of symphysis	27. 2	?	*23. 15	?
Height below M2	*13. 8	10. 56	15. 7	14. 9
Transverse width below M1	?	?	7. 9	?
Transverse width below M2	?	5. 6		7. 5

Supplementary figures S1-5

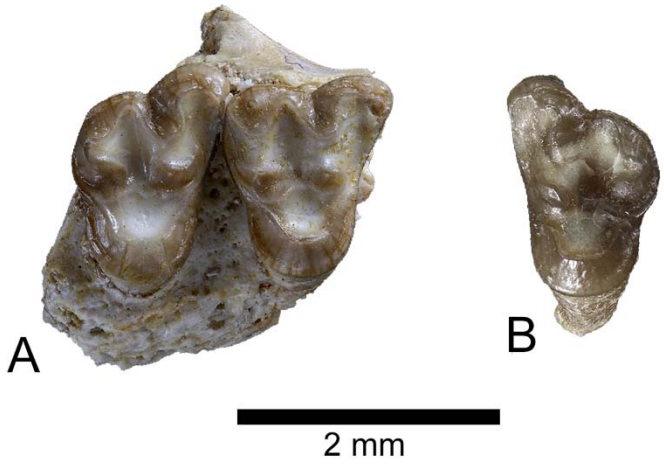

FIGURE S1. *Hadrogeneios phosphaticus* n. g., n. sp. MHNM.KHG.226. **A**, fragment of right maxillary bearing strongly worn M2-3; **B**, isolated left M3 of the same individual. Occlusal views. Scale in millimeters.

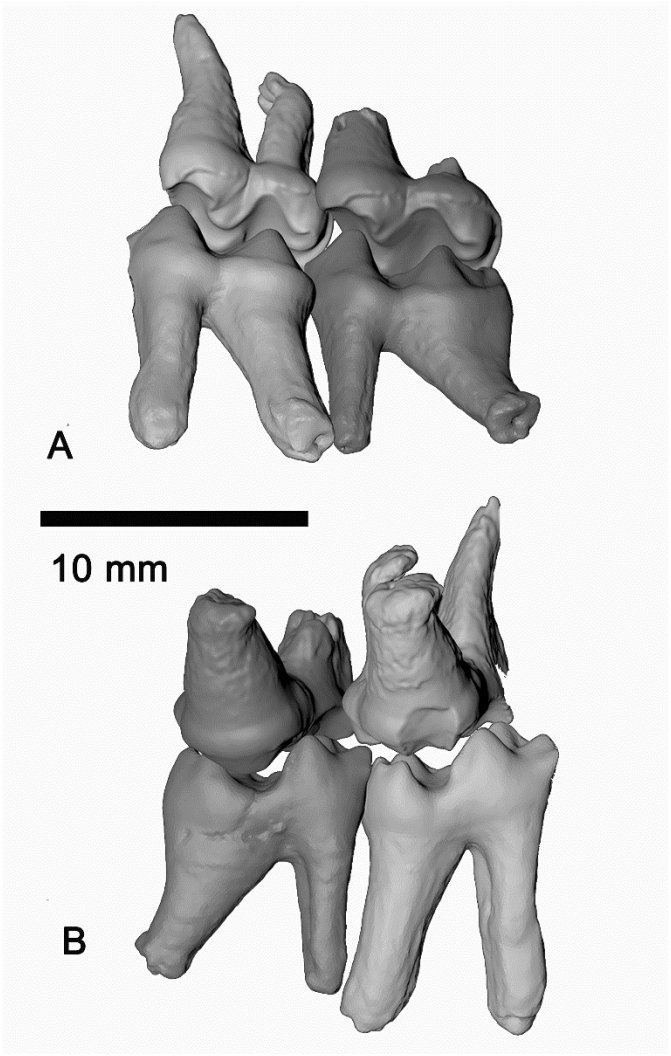

Figure S2. *Hadrogeneios phosphaticus* n. g., n. sp. Reconstruction of the molar occlusion based on the 3D digital models made from the CT scans of specimens MHNM.KHG.226 (right M2-M3 in reversed view) and MHNM.KHG.225 (left m2-3). Ventrolabial and lingual views. The specimen MHNM.KHG.226 is here enlarged by about 10% to adjust the precise molar occlusion with MHNM.KHG.225, which belongs to a slightly larger individual.

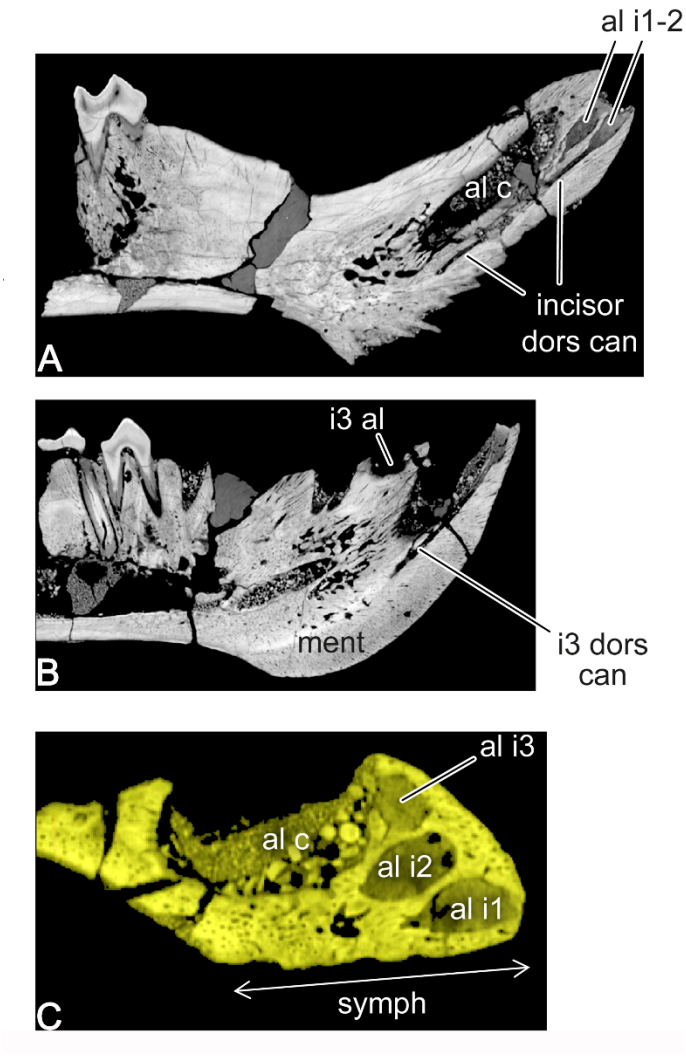

FIGURE S3. *Hadrogeneios phosphaticus* n. g., n. sp. CT scan sections of the dentary MHNM.KHG.224 showing the alveoli of the incisors and their neurovascular canaliculi. **A-B**, longitudinal (sagittal) section showing the alveoli of i1-3 and their thin dorsal canaliculus; b also shows the bifid alveolus of p1 (and posteriorly alveoli of p2, and the teeth p3 and p4). **C**, horizontal (axial) section showing the small alveoli of i1-3 and their relative position and development. **Abbreviations**: al: tooth alveolus; dors can: dorsal canaliculus; ment: mentum; symph: mandibular symphysis.

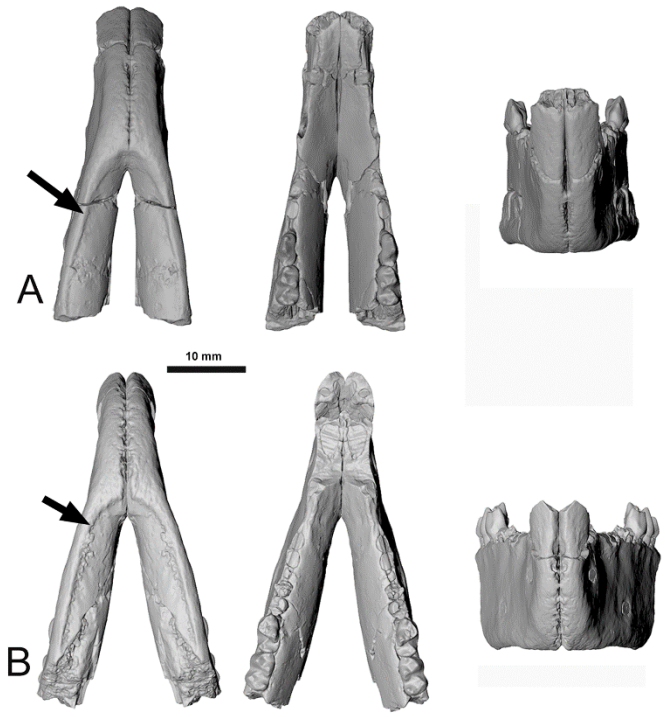

FIGURE S4. *Hadrogeneios phosphaticus* n. g., n. sp. 3D digital reconstruction by symmetrization of the mandibular symphyseal region. **A**, MHNM.KHG.224 in ventral, dorsal and anterior views. **B**, holotype MHNM.KHG.227 in ventral, dorsal and anterior views. The slight difference in the angle of the rami of MHNM.KHG.224 and MHNM.KHG.227 seen here is linked to postmortem deformation (preservation). Arrow: ventral bony crest for muscular attachment, probably for muscle genioglossus of the tongue.

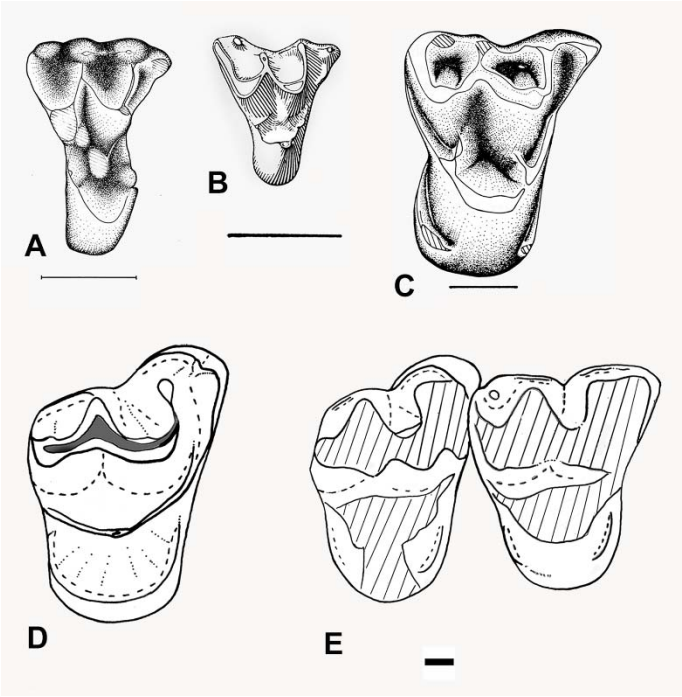

FIGURE S5. Comparison of the upper molar morphology of *Hadrogeneios phosphaticus* n. g., n. sp. with dilambdodont adapisoriculids *Garatherium* and *Remiculus*. **A**, *Garatherium* n. sp. from the Late Paleocene of Adrar Mgorn, Morocco; reversed view of THR362, M1 or M2 (fig. 12-2 in Gheerbrant, 1995). **B**, *Garatherium mahboubi* from the Ypresian of El Kohol, Algeria; holotype, M1 or M2 (fig. 1 in Crochet, 1984). **C**, *Remiculus deutschi* from the late Paleocene of Cernay-Berru, France; reversed view of holotype, M2 (fig. 12-5 in Gheerbrant, 1995). **D-E**, *Hadrogeneios phosphaticus* n. g., n. sp. D. Specimen MHNM.KHG.223, right M3. E. Specimen MHNM.KHG.226, right M2-3. Occlusal sketches made with camera lucida. Scale bar= 1 mm.

References

Crochet, J. Y. 1984. *Garatherium mahboubii* nov. gen., nov. sp., Marsupial de l'Eocène inférieur d'El Kohol (Sud Oranais, Algérie). Annales de Paléontologie (Vertébrés-Invertébrés) 70:275–294.

Gheerbrant, E. 1995. Les mammifères paléocènes du Bassin d'Ouarzazate (Maroc). III. Adapisoriculidae et autres mammifères (Carnivora, ?Creodonta, Condylarthra, ?Ungulata et *incertae sedis*). Palaeontographica A 237:39–132.

Journal of Vertebrate Paleontology

Supplementary data

Supplementary Information S1

Ancestral radiation of paenungulate mammals (Paenungulatomorpha) - new evidence from the Paleocene of Morocco

EMMANUEL GHEERBRANT

CNRS, CR2P (CNRS-MNHN-Sorbonne Université), Museum national d'Histoire naturelle, CP38, 57 rue Cuvier, F-75231 Paris cedex 05, France, emmanuel.gheerbrant@mnhn.fr

1. Studied characters

Our character matrix includes 38 taxa and 209 characters numbered starting from 0. It corresponds to that of Gheerbrant, (2009) and Gheerbrant *et al.* (2021) with a few corrections and additions**.** The main changes with respect to Gheerbrant *et al.* (2021) correspond the replacement of the taxon Sirenia by the following three stem genera: *Prorastomus*, *Pezosiren*, and *Eotheroides*. Their coding, especially for *Pezosiren*, was made from Domning (2001), Domning et al. (2017), and Domning (in press).

Other minor changes were made :

- Character 6: state 0 redefined: I/2 “not enlarged” (states for proboscideans recoded 0, except for *Moeritherium*).
- Character 186 (mastoidy/amastoidy): in sirenians there is a mastoid exposure on the occiput, but it is a secondary state (Novacek and Wyss, 1987).
- Character 209 is added to account for the presence of surnumerary premolar (P5 and dP5) in stem sirenians.

The character matrix, including character list and description, is provided in Supplementary File (Nexus file).

2. Character matrix for *Hadrogeneios*

Matrix

The matrix includes 9 characters that are uninformative (4, 5, 63, 73, 102, 132, 178, 190, 199).

Taxa analysed

The basal out-group taxon (Eutheria) corresponds to the generalized eutherian morphotype.

38 terminal taxa

0 Eutheria (out-group)
1 *Abdounodus*
2 Anthracobunidae
3 Arctocyonidae
4 *Barytherium*
5 *Cambaytherium*
6 Desmostylia
7 *Eritherium*
8 *Eotherioides*
9 Hyopsodus
10 Hyracoidea
11 Macroscelidea
12 *Minchenella*
13 *Moeritherium*
14 *Numidotherium*
15 *Ocepeia*
16 *Orycteropus*
17 *Paschatherium*
18 Perissodactyla
19 *Pezosiren*
20 Phenacodontidae
21 *Phenacolophus*
22 *Phosphatherium*
23 *Potamogale*
24 Prorastomus
25 *Protungulatum*
26 *Ptolemaia*
27 *Radinskya*
28 *Teilhardimys*
29 *Todralestes*
30 *S. minor*
31 *Stylolophus major*
32 *Palaeoamasia*
33 *Hypsamasia*
34 *Crivadiatherium*
35 *Namatherium*
36 *Ars zitelli*
37 *Hadrogeneios*

Suprageneric taxa included in the matrix are coded on the basis of the most plesiomorphic genera included, by reference to the generalized morphotype of the group (see Gheerbrant, 2009). Their content follows Gheerbrant (2009): Eutheria corresponds to generalized eutherian morphotype represented by *Acristatherium*, *Prokennalestes*, *Asioryctes*, *Maelestes*, and *Cimolestes*; Arctocyonidae is based on *Loxolophus*, *Tricentes*, *Lambertocyon*, and *Chriacus*; Perissodactyla was coded based on the primitive perissodactyls *Hyracotherium*, *Cymbalophus*, *Pachynolophus*; Hyracoidea was coded based on the primitive hyracoids *Seggeurius*, *Microhyrax*, *Dimaitherium*, and *Saghatherium*. Anthracobunidae is based on *Anthracobune*; Desmostylia is based on *Behemetops* and *Ashoroa*; Phenacolophidae is based on *Phenacolophus* and *Minchenella*; Phenacodontidae is based on *Ectocion* and *Phenacodus*; Macroscelidea is based on primitive herodotine genera *Chambius* and *Herodotius* and on the extant genera *Petrodromus* and *Rhynchocyon*.

3. TNT analysis, method, cladograms, and characters at nodes

The parsimony analysis was developed using TNT 1.5 software. All analyses used the "traditional search" command with the option of Collapsing Branches with no possible support ("rule 3"). Bremer indices were calculated for 10000 trees with additional 10 steps longer than in the shortest obtained tree. The nine uninformative characters were made inactive before the analysis (command xinact). The interface WINCLADA associated with the heuristic algorithm NONA was used in complement of our study, especially for the revision of the matrix, for the preliminary explorative analysis of tree topology and for examination of character distribution in trees. Characters are numbered starting from 0 (default option of TNT and Winclada).
48 characters are treated as additive: 7, 11, 13, 27, 32, 35, 42, 43, 49, 50, 55, 58, 62, 63, 65, 68, 69, 75, 78, 86, 89, 93, 95, 104, 108, 109, 111, 113, 115, 116, 118, 119, 120, 122, 123, 128, 137, 138, 143, 149, 150, 154, 157, 158, 161, 182, 183, 192, 201.

Analysis 1: standard analysis (unweighted, unconstrained)

Strict consensus of 180 trees (0 taxa excluded; two rounds of TBR analysis).

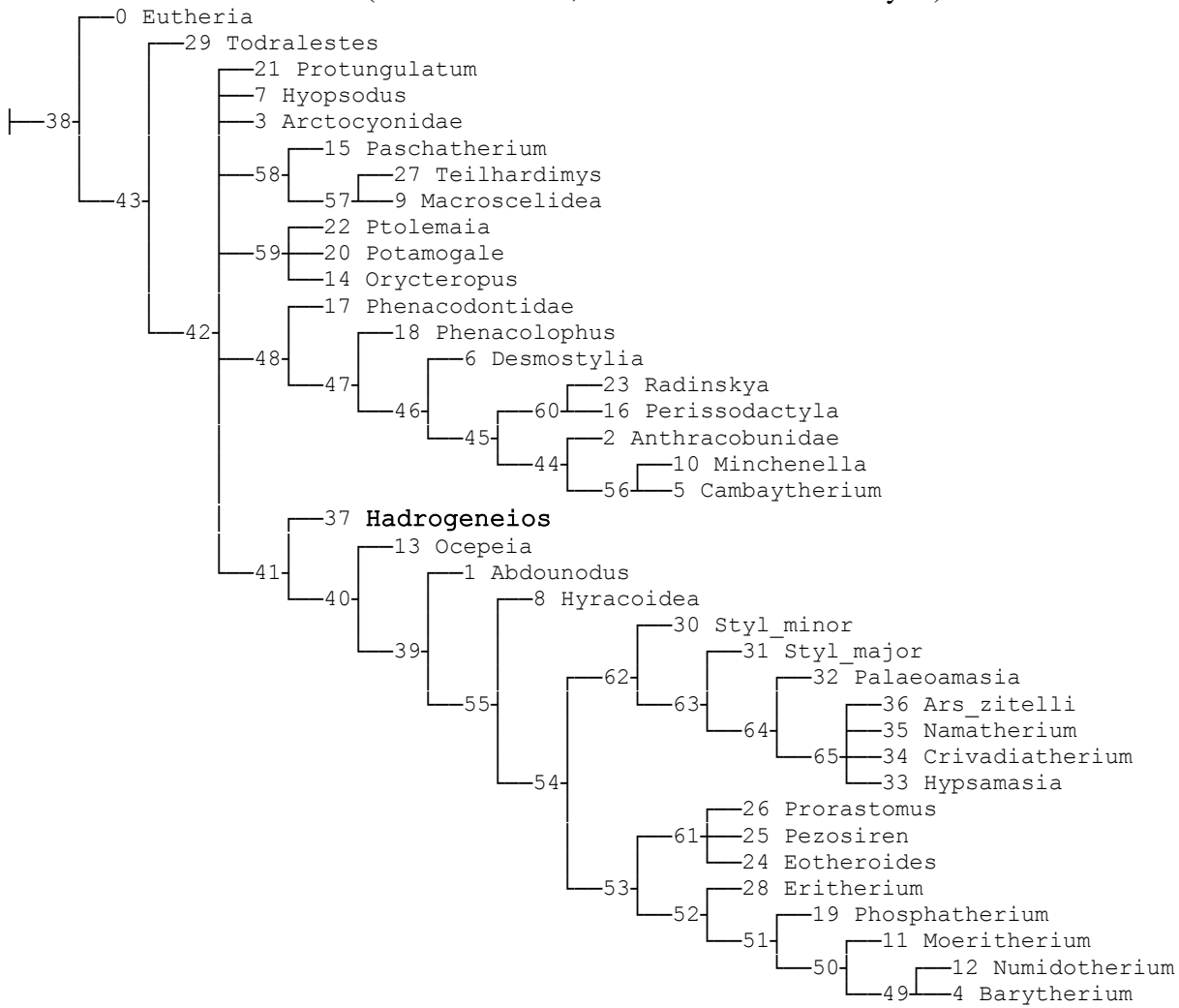

Tree lengths: 972. Retention index: 61.3. Consistency Index: 34.8.

Majority rule tree (from 180 trees, cut 50)

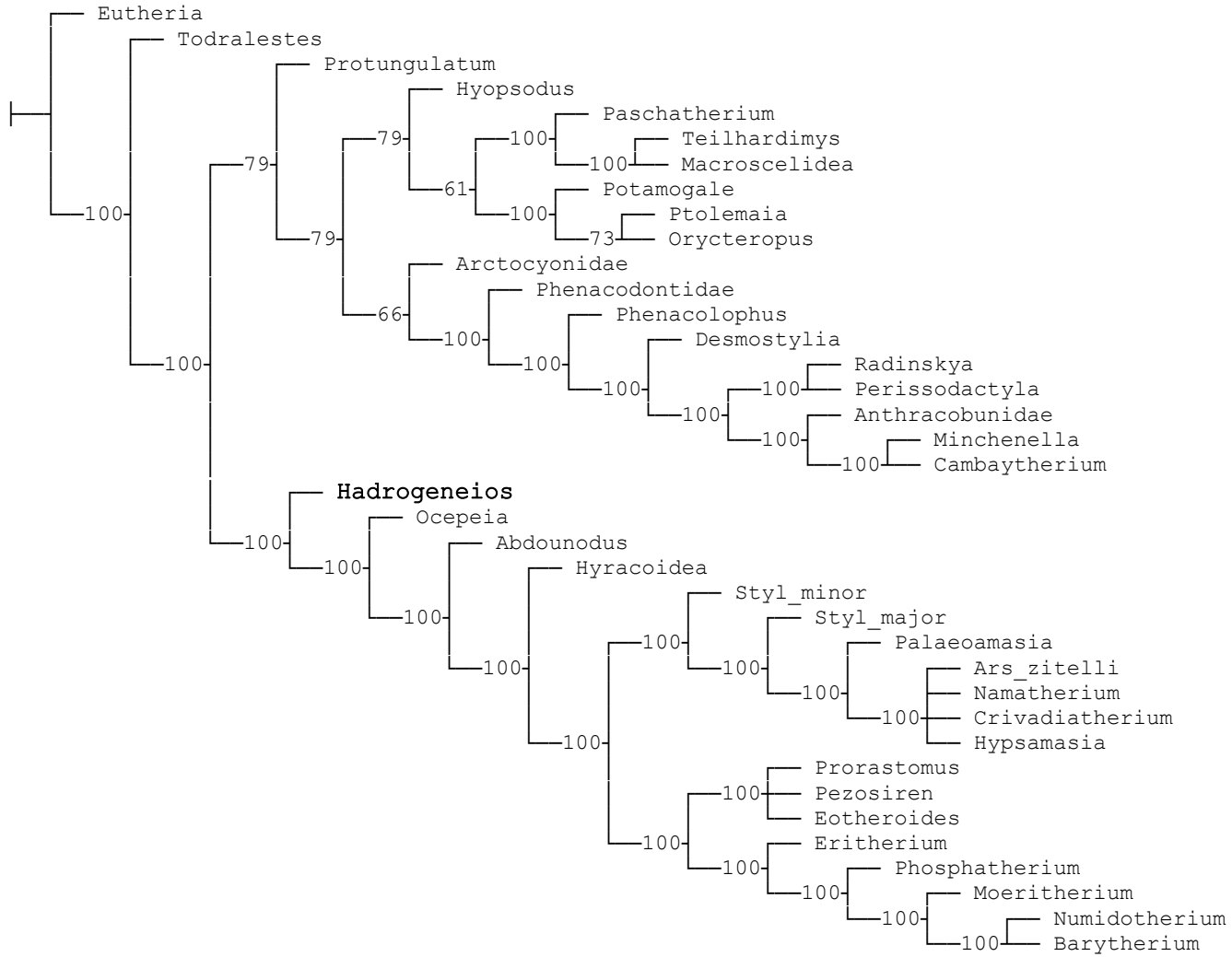

Synapomorphies common to 180 trees of the standard analysis

(Node numbers refer to nodes in consensus)

Eutheria :
All trees:
No autapomorphies:

Abdounodus :
All trees:
Char. 19: 1 --> 0
Char. 32: 12 --> 0
Char. 39: 1 --> 2
Char. 41: 0 --> 2
Char. 42: 0 --> 1
Char. 43: 1 --> 2
Char. 45: 1 --> 0
Char. 50: 02 --> 1
Char. 98: 0 --> 1
Char. 111: 0 --> 1
Char. 164: 1 --> 2

Anthracobunidae :
All trees:
Char. 26: 1 --> 2
Char. 165: 1 --> 0
Char. 193: 0 --> 1
Some trees:
Char. 58: 2 --> 1

Arctocyonidae :
All trees:
Char. 72: 0 --> 1
Char. 174: 0 --> 1
Some trees:
Char. 31: 0 --> 1
Char. 46: 1 --> 2
Char. 155: 0 --> 1
Char. 156: 2 --> 1
Char. 180: 0 --> 1
Char. 196: 1 --> 0
Char. 197: 2 --> 0
Char. 204: 0 --> 2

Barytherium :
All trees:
Char. 34: 1 --> 3
Char. 55: 1 --> 2
Char. 57: 0 --> 2
Char. 63: 0 --> 1
Char. 69: 1 --> 2
Char. 77: 1 --> 3
Char. 79: 1 --> 0
Char. 125: 1 --> 0
Char. 164: 1 --> 3

Cambaytherium :
All trees:
Char. 16: 1 --> 0
Char. 18: 1 --> 0
Char. 21: 0 --> 1
Char. 22: 1 --> 0
Char. 23: 1 --> 0
Char. 25: 2 --> 1
Char. 39: 0 --> 2

Desmostylia :
All trees:
Char. 0: 0 --> 1
Char. 1: 0 --> 1
Char. 8: 1 --> 0
Char. 17: 0 --> 1
Char. 32: 2 --> 0
Char. 61: 1 --> 2
Char. 64: 0 --> 1
Char. 84: 3 --> 0
Char. 91: 0 --> 1
Char. 107: 0 --> 1
Char. 108: 0 --> 3
Char. 109: 1 --> 3
Char. 112: 0 --> 1
Char. 115: 12 --> 0
Char. 118: 1 --> 2
Char. 145: 0 --> 1
Char. 147: 0 --> 1
Char. 154: 1 --> 23
Char. 157: 1 --> 3
Char. 161: 0 --> 12
Char. 164: 1 --> 34
Char. 181: 0 --> 1
Some trees:
Char. 58: 2 --> 1
Char. 155: 0 --> 1

Hyopsodus :
All trees:
Char. 13: 0 --> 1
Char. 176: 0 --> 1
Char. 183: 0 --> 1
Char. 188: 0 --> 1
Char. 193: 0 --> 1
Some trees:
Char. 6: 0 --> 1
Char. 11: 1 --> 2
Char. 22: 0 --> 1
Char. 36: 0 --> 1
Char. 39: 1 --> 0
Char. 41: 0 --> 1
Char. 58: 2 --> 1
Char. 72: 0 --> 1
Char. 115: 1 --> 2
Char. 140: 0 --> 2
Char. 161: 0 --> 1

Hyracoidea :
All trees:

Char. 16: 0 --> 1
Char. 31: 1 --> 0
Char. 44: 0 --> 1
Char. 51: 0 --> 1
Char. 74: 0 --> 1
Char. 75: 0 --> 2
Char. 88: 0 --> 1
Char. 120: 1 --> 2
Char. 166: 0 --> 1
Char. 170: 0 --> 1
Char. 173: 0 --> 12
Char. 194: 0 --> 2
Char. 201: 2 --> 1

Macroscelidea :
All trees:
Char. 22: 0 --> 1
Char. 24: 0 --> 1
Char. 46: 1 --> 0
Char. 50: 0 --> 1
Char. 84: 2 --> 3
Char. 87: 1 --> 0
Char. 164: 1 --> 2
Some trees:
Char. 17: 1 --> 0
Char. 29: 1 --> 0
Char. 32: 0 --> 1

Minchenella :
All trees:
Char. 41: 0 --> 1
Char. 54: 0 --> 1
Char. 98: 1 --> 0
Char. 99: 1 --> 0
Char. 109: 1 --> 0
Char. 110: 1 --> 0
Char. 111: 1 --> 0
Char. 117: 2 --> 1
Char. 118: 1 --> 0
Char. 120: 1 --> 2
Some trees:
Char. 46: 1 --> 0

Moeritherium :
All trees:
Char. 2: 0 --> 1
Char. 6: 0 --> 1
Char. 21: 1 --> 0
Char. 25: 3 --> 4
Char. 27: 0 --> 2
Char. 31: 1 --> 0
Char. 42: 1 --> 2
Char. 57: 0 --> 1
Char. 67: 0 --> 1
Char. 70: 1 --> 0
Char. 76: 0 --> 2
Char. 79: 1 --> 3
Char. 80: 0 --> 1
Char. 84: 1 --> 3
Char. 85: 0 --> 1
Char. 87: 0 --> 1
Char. 95: 3 --> 4
Char. 114: 0 --> 2
Char. 145: 0 --> 1
Char. 153: 0 --> 1
Char. 154: 2 --> 3
Char. 156: 2 --> 3
Char. 161: 1 --> 2
Char. 164: 1 --> 5
Char. 165: 0 --> 1
Char. 171: 0 --> 1
Char. 172: 0 --> 1
Char. 191: 0 --> 1
Char. 203: 0 --> 1

Numidotherium :
All trees:
No autapomorphies:

Ocepeia :
All trees:
Char. 7: 0 --> 1
Char. 11: 12 --> 3
Char. 13: 0 --> 3
Char. 41: 0 --> 1
Char. 45: 1 --> 2
Char. 47: 0 --> 1
Char. 51: 0 --> 1
Char. 52: 0 --> 3
Char. 66: 0 --> 1
Char. 67: 0 --> 1
Char. 68: 0 --> 1
Char. 71: 0 --> 1
Char. 137: 0 --> 2
Char. 140: 0 --> 3
Char. 172: 0 --> 1
Char. 187: 0 --> 1
Char. 188: 0 --> 1
Char. 203: 0 --> 1
Some trees:
Char. 117: 1 --> 0
Char. 127: 1 --> 3
Char. 151: 1 --> 0
Char. 154: 1 --> 0

Orycteropus :
All trees:
Char. 10: 0 --> 12
Char. 13: 0 --> 2
Char. 14: 0 --> 1
Char. 15: 0 --> 1
Char. 20: 0 --> 1
Char. 57: 0 --> 2
Char. 63: 0 --> 3
Char. 68: 0 --> 2
Char. 69: 01 --> 2
Char. 74: 0 --> 2
Char. 77: 1 --> 2
Char. 83: 1 --> 3
Char. 135: 0 --> 1
Char. 139: 0 --> 1
Char. 141: 0 --> 1
Char. 147: 0 --> 1
Char. 160: 0 --> 2
Char. 183: 0 --> 2
Some trees:
Char. 2: 0 --> 1
Char. 8: 3 --> 5
Char. 45: 1 --> 2
Char. 58: 01 --> 2
Char. 61: 0 --> 1
Char. 159: 1 --> 0

Char. 164: 1 --> 0
Char. 179: 1 --> 0
Char. 192: 0 --> 2
Char. 194: 1 --> 2
Char. 203: 1 --> 0

Paschatherium :
All trees:
Char. 11: 1 --> 0
Char. 12: 1 --> 0
Char. 25: 1 --> 0
Char. 81: 1 --> 0
Char. 92: 1 --> 0
Char. 98: 1 --> 0
Some trees:
Char. 39: 1 --> 2

Perissodactyla :
All trees:
Char. 76: 0 --> 2
Char. 118: 1 --> 2
Char. 139: 0 --> 1
Char. 146: 0 --> 1
Char. 151: 1 --> 0
Char. 154: 1 --> 0
Char. 180: 0 --> 1

Phenacodontidae :
All trees:
Char. 38: 0 --> 1
Char. 140: 0 --> 2
Char. 146: 0 --> 1
Char. 193: 0 --> 1
Some trees:
Char. 11: 1 --> 2
Char. 151: 1 --> 0
Char. 189: 1 --> 0

Phenacolophus :
All trees:
Char. 6: 0 --> 1
Char. 8: 1 --> 3
Char. 21: 0 --> 1
Char. 33: 0 --> 1
Char. 74: 0 --> 2
Char. 109: 1 --> 0
Char. 110: 1 --> 0
Char. 113: 01 --> 2
Char. 126: 1 --> 0
Char. 204: 1 --> 3
Some trees:
Char. 46: 1 --> 2

Phosphatherium :
All trees:
Char. 58: 2 --> 1
Char. 134: 0 --> 2
Char. 140: 0 --> 2

Potamogale :
All trees:
Char. 46: 1 --> 0
Char. 50: 0 --> 2
Char. 114: 0 --> 1
Char. 153: 0 --> 1
Char. 158: 0 --> 2
Char. 161: 01 --> 2
Char. 172: 0 --> 1
Char. 184: 0 --> 1
Some trees:
Char. 48: 1 --> 0
Char. 53: 0 --> 1
Char. 65: 1 --> 2
Char. 70: 1 --> 0
Char. 92: 1 --> 0
Char. 98: 1 --> 0
Char. 109: 1 --> 0
Char. 110: 1 --> 0
Char. 111: 1 --> 0
Char. 142: 0 --> 2
Char. 146: 0 --> 1
Char. 154: 12 --> 3
Char. 156: 0 --> 3
Char. 157: 0 --> 12
Char. 163: 0 --> 1
Char. 197: 0 --> 1
Char. 198: 0 --> 1
Char. 202: 0 --> 2
Char. 203: 01 --> 1

Protungulatum :
All trees:
Char. 28: 0 --> 1
Char. 46: 1 --> 0
Char. 47: 0 --> 2
Char. 61: 1 --> 2

Ptolemaia :
All trees:
Char. 126: 1 --> 2
Char. 127: 1 --> 2
Some trees:
Char. 8: 3 --> 0
Char. 17: 1 --> 0
Char. 52: 0 --> 2
Char. 64: 1 --> 0
Char. 69: 01 --> 0
Char. 78: 1 --> 2
Char. 84: 0 --> 1
Char. 171: 1 --> 0

Radinskya :
All trees:
Char. 84: 3 --> 1
Char. 164: 1 --> 0

Eotheroides :
All trees:
Char. 140: 0 --> 1
Char. 179: 1 --> 0
Some trees:
Char. 3: 1 --> 0
Char. 25: 2 --> 1
Char. 83: 1 --> 3
Char. 157: 3 --> 5
Char. 161: 1 --> 2
Char. 175: 0 --> 1

Pezosiren :
All trees:
Char. 172: 0 --> 1
Some trees:

Char. 194: 1 --> 2

Prorastomus :
All trees:
Char. 9: 1 --> 0
Char. 10: 0 --> 1
Char. 12: 1 --> 0
Char. 70: 1 --> 0
Some trees:
Char. 6: 0 --> 1
Char. 103: 0 --> 1

Teilhardimys :
All trees:
Char. 21: 0 --> 1
Char. 26: 0 --> 2
Char. 74: 0 --> 1
Char. 75: 0 --> 2
Char. 114: 0 --> 1
Char. 120: 01 --> 2
Char. 121: 0 --> 1
Char. 135: 0 --> 12
Some trees:
Char. 36: 0 --> 1

Eritherium :
All trees:
Char. 42: 1 --> 2
Char. 48: 2 --> 1
Char. 50: 2 --> 0
Char. 100: 0 --> 1
Char. 101: 3 --> 2
Char. 127: 3 --> 1

Char. 192: 1 --> 0

Todralestes :
All trees:
Char. 52: 0 --> 3
Char. 53: 0 --> 1
Some trees:
Char. 10: 0 --> 1
Char. 93: 0 --> 1

Styl_minor :
All trees:
Char. 31: 1 --> 0
Char. 50: 2 --> 1
Char. 58: 2 --> 1
Char. 140: 0 --> 2

Styl_major :
All trees:
Char. 135: 1 --> 2

Palaeoamasia :
All trees:
Char. 10: 0 --> 1
Char. 54: 0 --> 1
Some trees:
Char. 87: 0 --> 1
Char. 91: 1 --> 0

Hypsamasia :
Some trees:
Char. 80: 0 --> 1
Char. 87: 0 --> 1

Char. 91: 1 --> 0

Crivadiatherium :
Some trees:
Char. 24: 0 --> 1
Char. 44: 0 --> 1
Char. 45: 1 --> 0

Namatherium :
Some trees:
Char. 88: 0 --> 1
Char. 100: 0 --> 1
Char. 145: 0 --> 2
Char. 164: 0 --> 2

Ars_zitelli :
Some trees:
Char. 49: 0 --> 2
Char. 83: 1 --> 0
Char. 84: 2 --> 3
Char. 89: 0 --> 2
Char. 103: 1 --> 0
Char. 108: 12 --> 3
Char. 123: 1 --> 2
Char. 127: 3 --> 0
Char. 128: 2 --> 3
Char. 135: 1 --> 2
Char. 156: 2 --> 3
Char. 157: 23 --> 01
Char. 160: 01 --> 2
Char. 162: 1 --> 0
Char. 205: 1 --> 2

Hadrogeneios :
All trees:
Char. 11: 1 --> 0
Char. 22: 0 --> 1
Char. 41: 0 --> 3
Char. 53: 0 --> 3
Char. 114: 0 --> 2
Some trees:
Char. 115: 1 --> 0
Char. 127: 1 --> 0

Node 39 :
All trees:
Char. 40: 0 --> 1
Char. 43: 0 --> 1
Char. 94: 0 --> 1
Char. 95: 0 --> 1
Char. 103: 1 --> 0
Char. 109: 0 --> 1
Char. 110: 0 --> 1
Char. 115: 2 --> 3
Char. 118: 0 --> 1
Char. 120: 0 --> 1
Char. 121: 0 --> 1
Char. 157: 0 --> 12

Node 40 :
All trees:
Char. 31: 0 --> 1
Char. 34: 0 --> 1
Char. 35: 0 --> 1
Char. 105: 0 --> 1
Char. 115: 01 --> 2

Char. 130: 0 --> 1

Node 41 (*Hadrogeneios* + Paenungulatomorpha) :
All trees:
Char. 38: 0 --> 1
Char. 55: 0 --> 1
Char. 62: 0 --> 1
Char. 104: 0 --> 1
Char. 113: 0 --> 2
Some trees:
Char. 10: 0 --> 1

Node 42 :
All trees:
Char. 25: 0 --> 1
Char. 126: 0 --> 1
Some trees:
Char. 32: 0 --> 1
Char. 92: 0 --> 1
Char. 117: 0 --> 1
Char. 127: 0 --> 1

Node 43 :
All trees:
No synapomorphies

Node 44 :
All trees:
Char. 11: 1 --> 0
Char. 43: 0 --> 2

Node 45 :
All trees:
Char. 16: 0 --> 1
Char. 152: 0 --> 1

Node 46 :
All trees:
Char. 28: 0 --> 1
Char. 29: 0 --> 1
Char. 30: 0 --> 1
Char. 124: 0 --> 1
Char. 157: 0 --> 1
Some trees:
Char. 36: 0 --> 1

Node 47 :
All trees:
Char. 26: 0 --> 1
Char. 34: 0 --> 1
Char. 35: 0 --> 1
Char. 40: 0 --> 2
Char. 78: 1 --> 2
Char. 97: 0 --> 2
Char. 127: 1 --> 3
Char. 135: 0 --> 2

Node 48 :
All trees:
Char. 32: 1 --> 2
Char. 79: 0 --> 2
Char. 82: 0 --> 1
Char. 84: 0 --> 3
Char. 93: 2 --> 3
Char. 120: 0 --> 1
Char. 121: 0 --> 1
Char. 165: 0 --> 1
Some trees:
Char. 22: 0 --> 1
Char. 128: 0 --> 1
Char. 142: 0 --> 2
Char. 204: 0 --> 1

Node 49 :
All trees:
Char. 13: 2 --> 0
Char. 38: 1 --> 0
Char. 39: 2 --> 1
Char. 42: 1 --> 0
Char. 43: 12 --> 0
Char. 68: 1 --> 2
Char. 137: 0 --> 1
Char. 204: 1 --> 2
Char. 207: 2 --> 3

Node 50 :
All trees:
Char. 10: 0 --> 3
Char. 11: 2 --> 3
Char. 14: 1 --> 0
Char. 18: 0 --> 1
Char. 22: 0 --> 1
Char. 51: 0 --> 1
Char. 54: 0 --> 1
Char. 56: 0 --> 1
Char. 68: 0 --> 1
Char. 71: 0 --> 1
Char. 74: 0 --> 1
Char. 75: 0 --> 1
Char. 104: 1 --> 0
Char. 107: 0 --> 1
Char. 108: 0 --> 3
Char. 141: 0 --> 1
Char. 148: 0 --> 1
Char. 158: 1 --> 2
Char. 175: 0 --> 1
Char. 182: 1 --> 2
Char. 198: 0 --> 1

Node 51 :
All trees:
Char. 3: 1 --> 2
Char. 7: 1 --> 2
Char. 8: 4 --> 5
Char. 25: 2 --> 3
Char. 32: 1 --> 0
Char. 45: 1 --> 2
Char. 46: 1 --> 2
Char. 90: 0 --> 1
Char. 95: 1 --> 3
Char. 120: 1 --> 23
Char. 135: 1 --> 2
Char. 157: 3 --> 4
Char. 162: 0 --> 1
Char. 188: 0 --> 1
Char. 202: 1 --> 0
Char. 204: 0 --> 1
Char. 207: 0 --> 2

Node 52 :
All trees:

Char. 7: 0 --> 1
Char. 39: 1 --> 2
Char. 41: 0 --> 2

Node 53 :
All trees:
Char. 98: 0 --> 1
Char. 155: 0 --> 1

Node 54 :
All trees:
Char. 40: 1 --> 2
Char. 72: 0 --> 1
Char. 91: 0 --> 1
Char. 100: 1 --> 0
Char. 118: 1 --> 2
Char. 157: 12 --> 3
Char. 161: 0 --> 1
Char. 181: 0 --> 1
Char. 183: 0 --> 12
Some trees:
Char. 127: 1 --> 3
Char. 159: 0 --> 1

Node 55 :
All trees:
Char. 10: 1 --> 0
Char. 25: 1 --> 2
Char. 26: 0 --> 2
Char. 28: 0 --> 1
Char. 29: 0 --> 1
Char. 30: 0 --> 1
Char. 48: 0 --> 2
Char. 58: 1 --> 2
Char. 79: 0 --> 1
Char. 84: 0 --> 2
Char. 97: 0 --> 1
Char. 115: 3 --> 4
Char. 116: 1 --> 2
Char. 128: 0 --> 1
Char. 131: 0 --> 1
Char. 133: 0 --> 1
Char. 135: 0 --> 1
Some trees:
Char. 81: 2 --> 1

Node 56 :
All trees:
Char. 17: 0 --> 1
Char. 45: 2 --> 0
Char. 124: 1 --> 0

Node 57 :
All trees:
Char. 37: 0 --> 1
Char. 40: 0 --> 1
Char. 78: 1 --> 2
Char. 93: 2 --> 3
Char. 94: 0 --> 1
Char. 95: 0 --> 1
Char. 128: 0 --> 1
Char. 134: 0 --> 1
Some trees:
Char. 19: 0 --> 1
Char. 27: 0 --> 1

Node 58 :
All trees:
Char. 79: 0 --> 1
Char. 84: 0 --> 2
Char. 127: 1 --> 2
Some trees:
Char. 48: 0 --> 1
Char. 53: 0 --> 1

Node 59 :
All trees:
Char. 71: 0 --> 1
Char. 155: 0 --> 1
Some trees:
Char. 11: 12 --> 3
Char. 44: 1 --> 0
Char. 59: 0 --> 1
Char. 86: 2 --> 1
Char. 87: 1 --> 0
Char. 93: 2 --> 0
Char. 103: 1 --> 0
Char. 115: 1 --> 0
Char. 140: 0 --> 1
Char. 145: 0 --> 1
Char. 156: 2 --> 0
Char. 167: 0 --> 1
Char. 175: 0 --> 1

Node 60 :
All trees:
Char. 95: 1 --> 2
Char. 120: 1 --> 2
Char. 127: 3 --> 1
Char. 135: 2 --> 0
Char. 184: 0 --> 1

Node 61 :
All trees:
Char. 20: 0 --> 1
Char. 51: 0 --> 1
Char. 54: 0 --> 1
Char. 148: 0 --> 1
Char. 149: 0 --> 2
Char. 150: 0 --> 2
Char. 208: 0 --> 1
Some trees:
Char. 15: 0 --> 1
Char. 61: 1 --> 2
Char. 68: 0 --> 1
Char. 74: 0 --> 2
Char. 77: 1 --> 2
Char. 164: 1 --> 2
Char. 194: 0 --> 1

Node 62 :
All trees:
Char. 25: 2 --> 3
Char. 33: 0 --> 1
Char. 35: 1 --> 2
Char. 38: 1 --> 0
Char. 39: 1 --> 0
Char. 41: 0 --> 1
Char. 55: 1 --> 0
Char. 67: 0 --> 1
Char. 81: 1 --> 0
Char. 96: 0 --> 1

Char. 103: 0 --> 1
Char. 104: 1 --> 2
Char. 107: 0 --> 2
Char. 110: 1 --> 0
Char. 113: 2 --> 3
Char. 114: 0 --> 2
Char. 119: 0 --> 1
Char. 122: 0 --> 1
Char. 123: 0 --> 1
Char. 136: 0 --> 1

Char. 143: 0 --> 1

Node 63 :
All trees:
Char. 108: 0 --> 1
Char. 109: 1 --> 2
Char. 162: 0 --> 1

Node 64 :
All trees:
Char. 74: 0 --> 1
Char. 75: 0 --> 1
Char. 76: 0 --> 2
Char. 128: 1 --> 2
Char. 129: 0 --> 1
Char. 164: 1 --> 0

Node 65 :
Some trees:
Char. 48: 2 --> 0

Char. 75: 1 --> 2
Char. 109: 2 --> 3
Char. 119: 1 --> 2
Char. 122: 1 --> 2
Char. 143: 1 --> 2
Char. 204: 0 --> 1
Char. 205: 0 --> 1

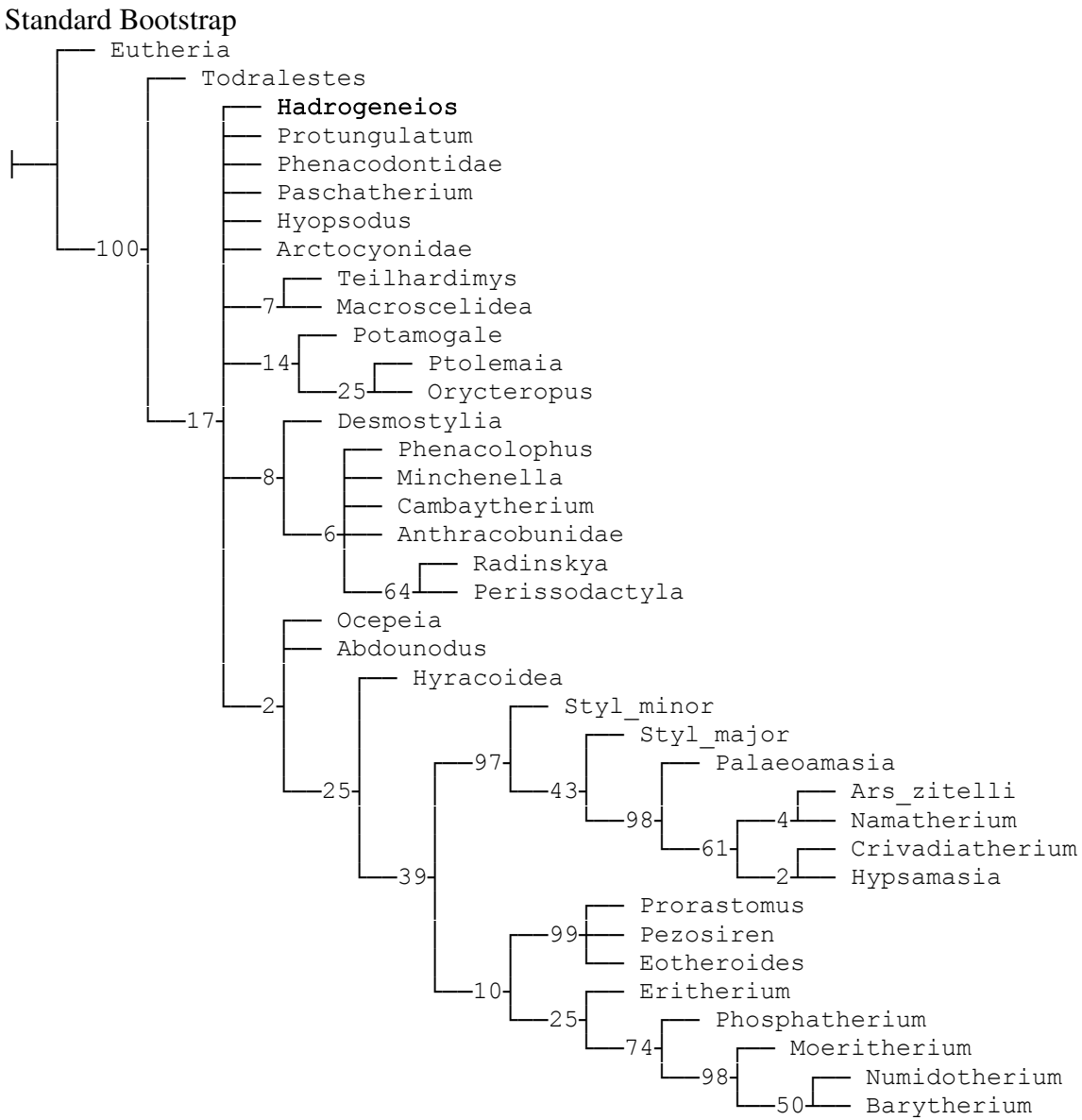
Standard Bootstrap
Eutheria
Todralestes
Hadrogeneios
Protungulatum
Phenacodontidae
Paschatherium
Hyopsodus
Arctocyonidae
Teilhardimys
Macroscelidea
Potamogale
Ptolemaia
Orycteropus
Desmostylia
Phenacolophus
Minchenella
Cambaytherium
Anthracobunidae
Radinskya
Perissodactyla
Ocepeia
Abdounodus
Hyracoidea
Styl_minor
Styl_major
Palaeoamasia
Ars_zitelli
Namatherium
Crivadiatherium
Hypsamasia
Prorastomus
Pezosiren
Eotheroides
Eritherium
Phosphatherium
Moeritherium
Numidotherium
Barytherium
100
7
14
25
17
8
6
64
2
25
97
43
98
4
61
2
39
99
10
25
74
98
50

Analysis 2: Clade Afrotheria constrained

In this analysis the following taxa are constrained to gather in the same clade Afrotheria: 1 *Abdounodus*; 4 *Barytherium*; 8 *Hyracoidea*; 9 *Macroscelidea*; 11 *Moeritherium*; 12 *Numidotherium*; 13 *Ocepeia*; 14 *Orycteropus*; 19 *Phosphatherium*; 20 *Potamogale*; 24 *Eotheroides*; 25 *Pezosiren*; 26 *Prorastomus*; 28 *Eritherium*; 30 *Stylophus_minor*; 31 *Stylophus _major*; 32 *Palaeoamasia*; 33 *Hypsamasia*; 34 *Crivadiatherium*; 35 *Namatherium*; 36 *Arsinoitherium zitelli*.
The used TNT command was: force +[1 4 8 9 11 12 13 14 19 20 24 25 26 28 30 31 32 33 34 35 36];constrain =;

1 - *Hadrogeneios* constrained to be included in Afrotheria.

Used TNT command: force +[1 4 8 9 11 12 13 14 19 20 24 25 26 28 30 31 32 33 34 35 36 37]; constrain =;

Strict consensus of 30 trees (0 taxa excluded), first round analysis

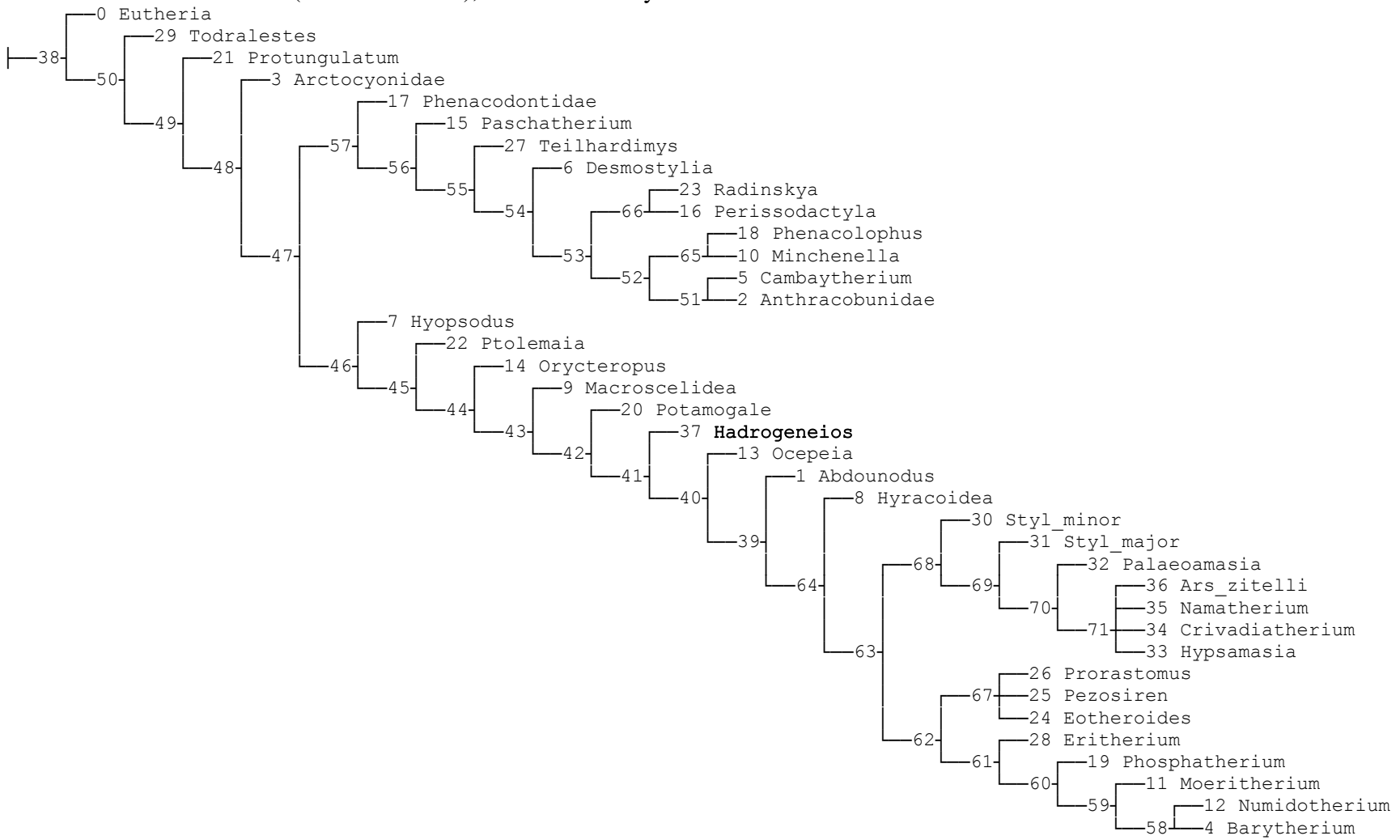

Tree lengths: 986. Retention index: 60.5. Consistency Index: 34.3.

Bremer supports (from 10000 trees, cut 2)

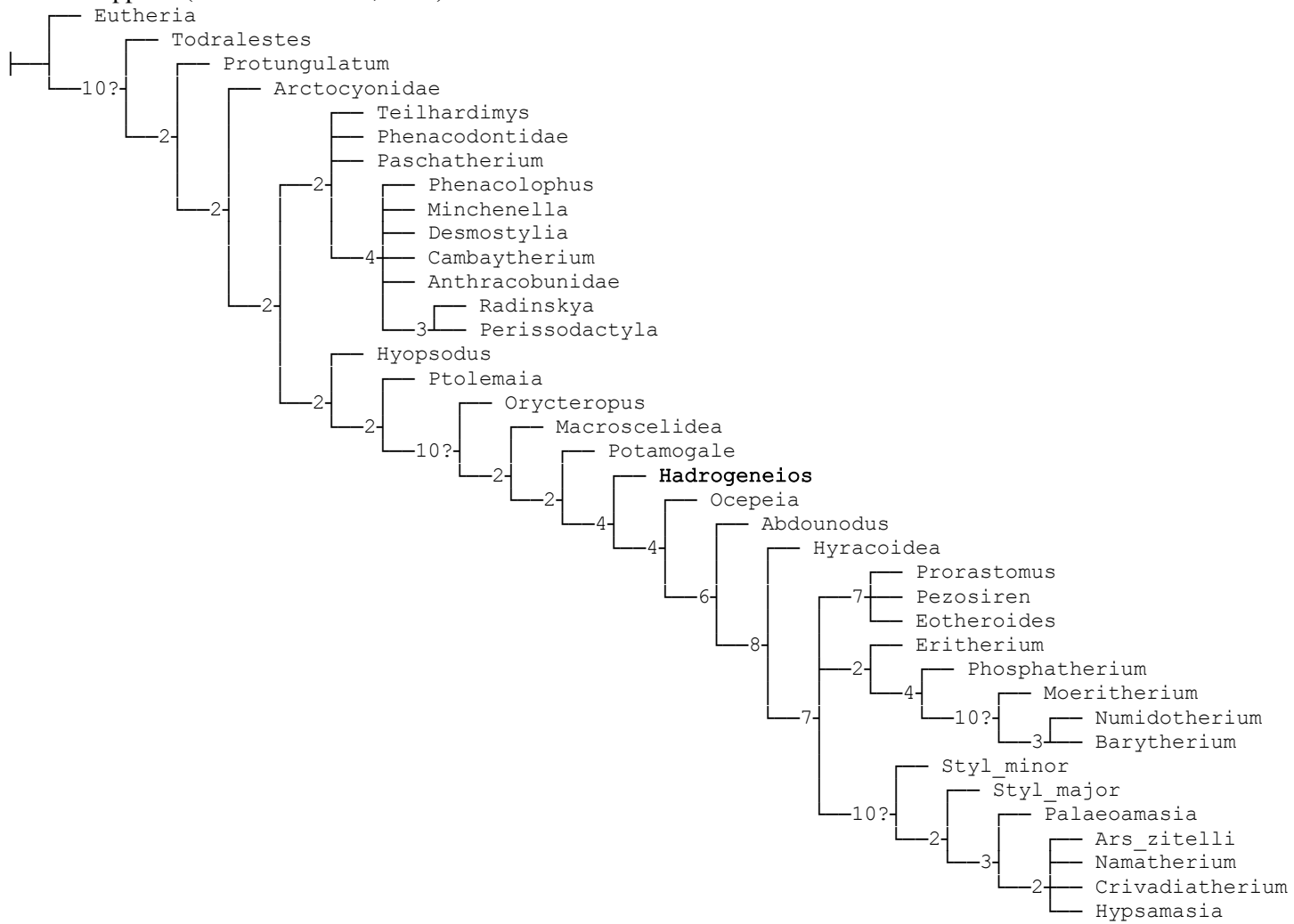

2 - *Hadrogeneios* position not constrained

Used command TNT: force +[1 4 8 9 11 12 13 14 19 20 24 25 26 28 30 31 32 33 34 35 36];constrain =;

Strict consensus of 530 trees (two rounds of TBR analysis)

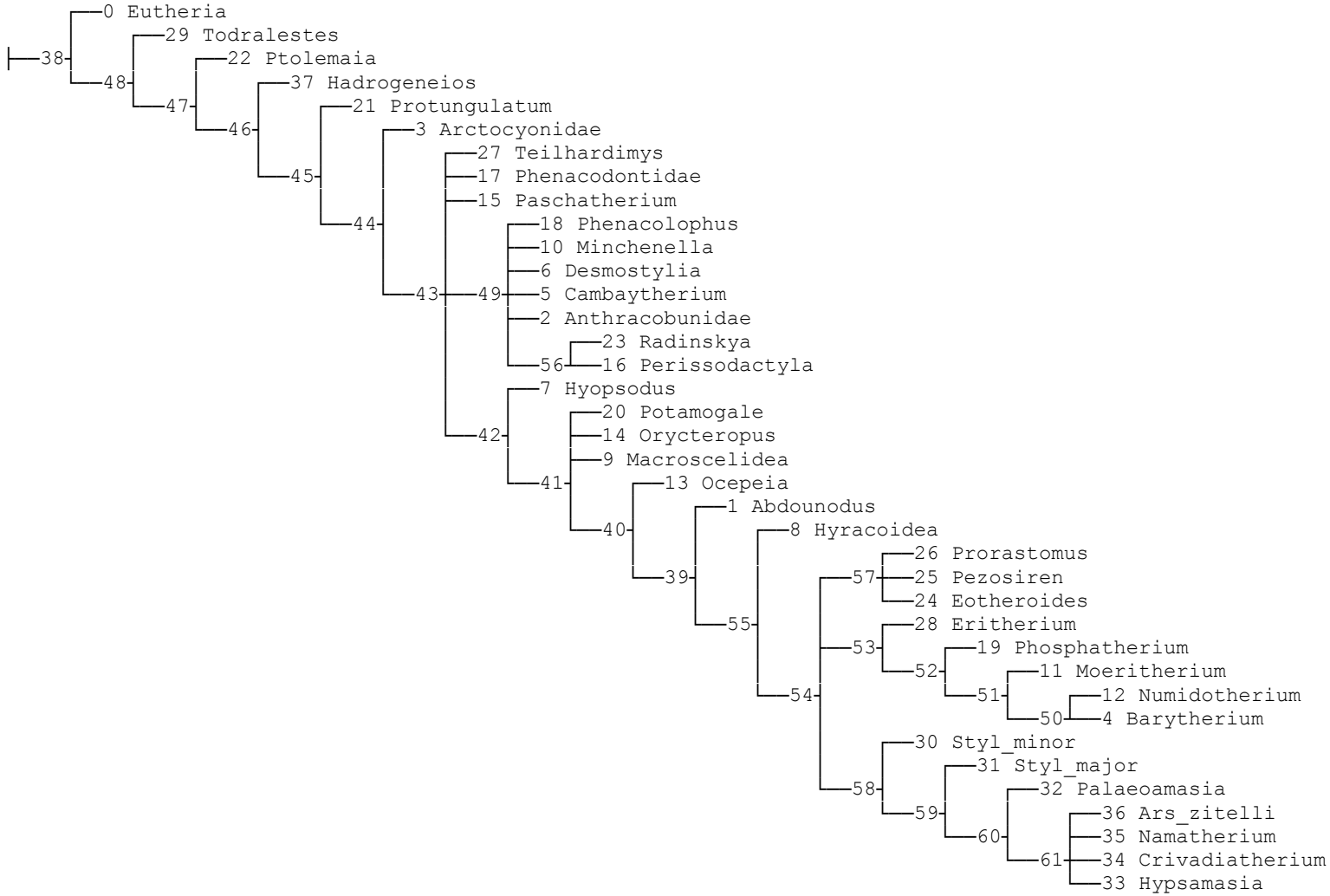

Tree lengths: 987. Retention index: 60.5. Consistency Index: 34.2.

Bremer support >2 (from 10000 trees, cut 2)

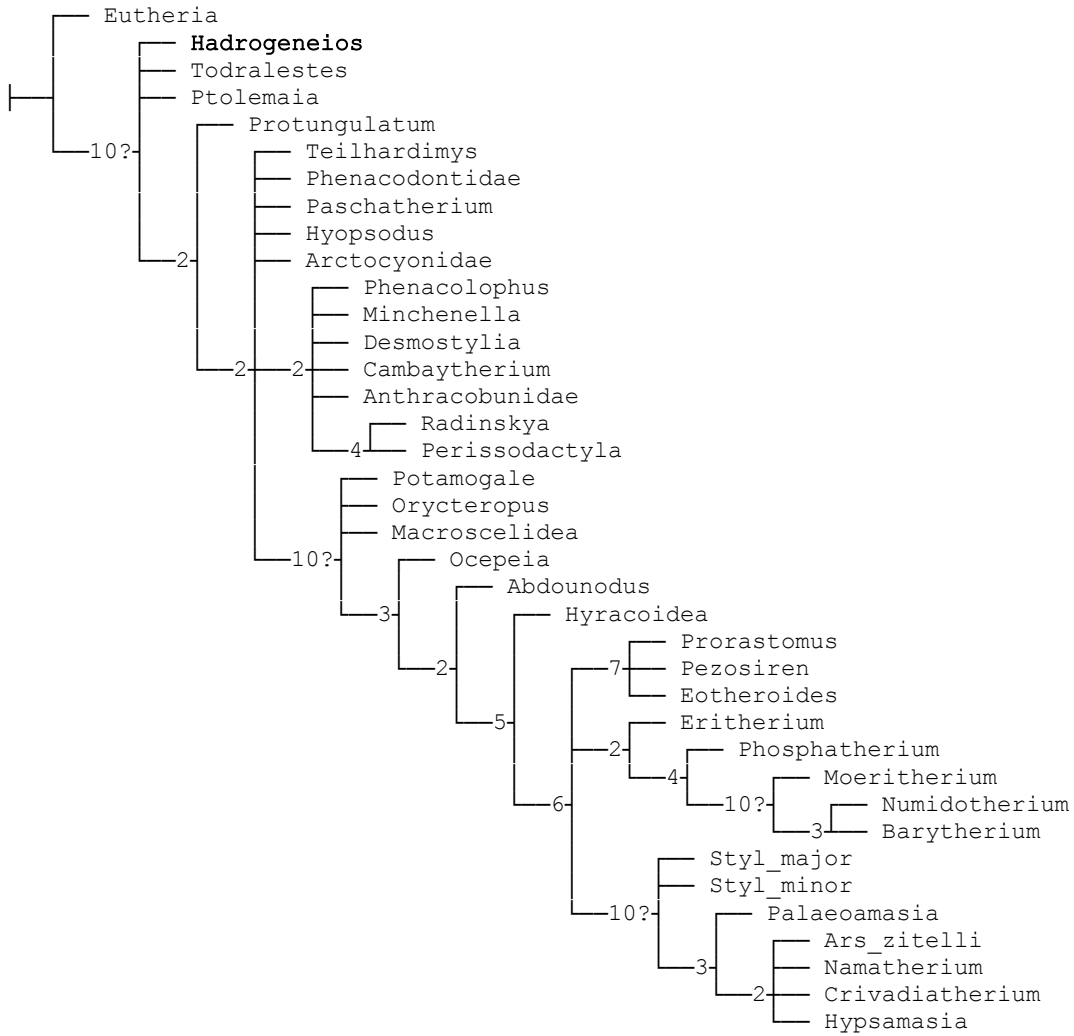

References

Domning, D. P. 2001. The earliest known fully quadrupedal sirenian. Nature 413:625–627.

Domning, D. P. in press. The Sirenia (Mammalia: Prorastomidae) of the Eocene Seven Rivers site, Jamaica; pp. in R. W. Portell and D. P. Domning (eds.), The Sirenia (Mammalia: Prorastomidae) of the Eocene Seven Rivers site, Jamaica, Springer.

Domning, D. P., G. J. Heal, and S. Sorbi. 2017. *Libysiren sickenbergi,* gen. et sp. nov.: a new sirenian (Mammalia, Protosirenidae) from the middle Eocene of Libya. Journal of Vertebrate Paleontology 37:e1299158.

Gheerbrant, E. 2009. Paleocene emergence of elephant relatives and the rapid radiation of African ungulates. Proceedings of the National Academy of Sciences 106:10717–10721.

Novacek, M. J., and A. R. Wyss. 1987. Selected Features of the Desmostylian Skeleton and Their Phylogenetic Implications. American Museum Novitates, 8:1-8.